School of Civil and Mechanical Engineering

Using KDamper for Seismic-Induced Vibration Mitigation of Wind Turbines

Xunyi Pan

This thesis is presented for the Degree of

Master of Philosophy

of

Curtin University

February 2024

Declaration

To the best of my knowledge and belief, this thesis contains no material previously published by any other person except where due acknowledgment has been made.

This thesis contains no material which has been accepted for the award of any other degree or diploma in any university.

Signature:

Date: 08/02/2024

Abstract

Wind energy plays an indispensable role among various renewable energy sources due to its eco-friendly and low-cost features. Environmental factors, including wind, wave, and seismic activity, may induce vibrations that are beyond the acceptable level on wind turbines, potentially compromising their structural functionality and safety. Hence it is necessary to investigate and reduce the adverse vibrations caused by external excitations.

Numerous methods have been developed to mitigate the vibrations of wind turbine towers, including the implementation of passive vibration control devices such as tuned mass dampers (TMDs), tuned liquid column dampers (TLCDs), tuned liquid dampers (TLDs), etc. It should be noted that better control effectiveness of the above-mentioned control devices is normally achieved by using a large auxiliary mass. Furthermore, conventional control devices are normally installed at the top of the tower or within the nacelle. The restricted space within the tower and nacelle presents considerable challenges for the implementation of such devices, rendering the utilization of large-scale control mechanisms unfeasible for the mitigation of vibrations in wind turbine towers.

Recently, a novel vibration control device, termed KDamper, has been proposed. The integration of a negative stiffness element within the damper imparts exceptional vibration control characteristics and considerable promise for application in wind turbine vibration control. However, very limited studies on applying KDamper to wind turbine towers for vibration mitigation have been reported. Hence, it is essential to understand the effect of KDamper on reducing wind turbine responses.

This study firstly reviews the current vibration control techniques for wind turbines and their corresponding pros and cons. Then the concept of KDamper and the critical parameters that influence the dynamic response of KDamper are introduced, and the analytical solutions for the optimal negative stiffness and damping ratios are derived. The NREL 5 MW wind turbine is selected as the prototype structure, 10 different connecting configurations of applying

KDamper to the wind turbine model are considered, and the optimal parameters for each connecting configuration are calculated. The wind turbine tower's dynamic responses, governed by each connecting configuration of the KDamper, are examined in the frequency domain. A comparative analysis and discussion of the control effects on displacement and acceleration responses between the TMD and KDamper are also conducted when the wind turbine is subjected to a series of seismic ground motions. The robustness of the KDamper is further investigated with increased and decreased structural frequencies. The results indicate that the KDamper outperforms the TMD in reducing the displacement and acceleration responses under different seismic ground motions. The KDamper also exhibits superior robustness than the TMD counterpart against structural frequency variations.

Acknowledgement

First and foremost, I would like to express my deepest gratitude to my supervisors Associate Professor Wensu Chen, Associate Professor Kaiming Bi and Professor Hong Hao for their valuable advice, continuous support, enlightening guidance, and great patience during my MPhil journey.

I would like to thank and acknowledge the group members of the Centre for Infrastructure Monitoring and Protection (CIMP) at Curtin University, including Drs. Haoran Zuo, Huan Li, Zheng Peng, Ruisheng Ma, and Mr Zhixing Li for their comments and suggestions during my MPhil study.

I acknowledge the financial support from the Australian Research Council (ARC) via Australian Future Fellowship FT200100183 to carry out the research. I also gratefully acknowledge the financial support from Curtin Research Stipend Scholarship to support my MPhil study.

Last but not least, I would like to express my deepest gratitude to my family, for their unconditional love, constant encouragement and support.

Table of Contents

List of Figures

List of Tables

Charpter 1 Introduction

1.1 Background

With the depletion of fossil energy storage, wind energy shows its indispensability as a clean energy source. The growth and expansion of wind farms have experienced significant acceleration in the last decade, especially in recent years. According to the Global Wind Energy Council, the global wind turbine installation reached a total of 873 GW by the end of 2021, representing a 3,492% increase compared to 2011 [1].

Wind turbines, the device for extracting wind energy and converting it to electricity, have been built in various locations that are rich in wind resources. As a result, wind turbines are subjected to different kinds of environmental loadings, such as wind, wave, and earthquake. These external excitations can cause undesired vibration and jeopardize structural integrity and reduce the performance of wind turbines. Moreover, to maximise the efficiency of energy extraction, modern wind turbines are designed with tall towers, large rotors, and lightweight materials, which makes wind turbines vulnerable to these unfavourable vibrations. As an illustration, the latest NREL 5 MW three-bladed wind turbine has a rotor diameter of 126 m and a tower height of 87.6 m, with a maximum tower wall thickness of 0.027 m only [2]. It is therefore important to find proper methods to suppress these unfavourable vibrations caused by environmental loads, so that the functionality of wind turbines can be maintained, and the energy extraction efficiency can be maximized.

1.2 Research objective

The primary aim of this thesis is to employ KDamper, in combination with customized installation arrangements, to mitigate wind turbine tower vibrations when it is subjected to seismic excitations. To this end, both analytical analyses and numerical simulations are conducted. The specific purposes of this thesis are as follows:

(1) To propose using KDamper for wind turbine tower vibration control, reveal the

factors influencing its performance and its basic properties, and understand the dynamic performance of KDamper in the frequency domain with respect to different negative stiffness ratios and connecting configurations.

(2) To investigate the dynamic responses of the wind turbine tower, including the displacement responses, acceleration responses, and robustness, under various seismic ground motions through the implementation of different control strategies.

1.3 Research outline

This thesis comprises six chapters, and the outline is as follows:

Chapter 1 introduces the background, research objective, and research outline.

Chapter 2 provides a comprehensive review of the existing literature on the topic.

Chapter 3 reviews the concept of KDamper, and investigates the influences of different mechanical parameters, including mass ratio, damping ratio and negative stiffness ratio, on KDamper's dynamic performance. Optimal selections of these parameters are also conducted to reveal the basic properties of KDamper.

In Chapter 4, the NREL 5MW wind turbine is adopted as the investigated model for this research. The equations of motion of the system equipped with KDamper are derived, and the optimal parameters are obtained for different configurations.

In Chapter 5, the dynamic responses of the system are analyzed in both the frequency and time domains. The performance of optimized TMD and optimized KDamper with different setups are firstly compared in the frequency domain, and one configuration is further selected to perform the time domain analysis. Then, the effectiveness of TMD and KDamper, including in mitigating the displacement and acceleration responses, and the robustness of the system, are compared and discussed under different seismic excitations.

Chapter 6 presents the main conclusions and recommendations for future works.

Charpter 2 Literature review

2.1 Introduction

Excessive vibrations caused by external excitations can cause negative impact on the functionality of wind turbines, compromising the conversion of wind energy into electricity, reducing the lifespan of structural components, and in severe cases, resulting in the complete collapse of the wind turbine (see Figure 2-1 [3]). To guarantee the safety and operationality of wind turbines, various approaches have been developed to reduce and control the excessive vibrations. Comprehensive reviews on wind turbine vibration mitigation have been provided in [4, 5].

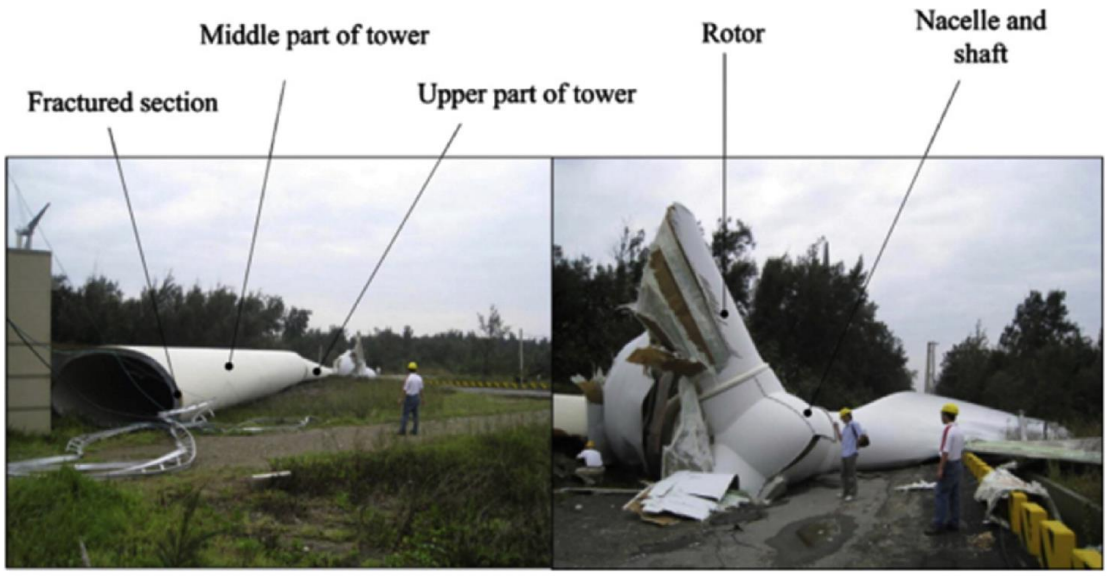

Figure 2-1. On-site photo of a collapsed wind turbine [3].

In this chapter, various control strategies for wind turbine vibration mitigation are reviewed, mainly focusing on passive control methods. In addition, the development of negative stiffness damper is presented and the existing studies on KDamper and its applications are reviewed.

2.2 Control strategies of wind turbines

A significant amount of research has been devoted to controlling the vibrations of wind turbine towers through the application of various control devices when the wind turbine is exposed to wind, wave, and seismic loads.

These methods can be generally categorised into three strategies, namely passive, active and semi-active. Active [6-8] and semiactive control [9-11] methods require external power input, which inevitably increases the complexity of the system. Therefore, they are less widely used in engineering practices compared to the passive control strategies.

The passive control approach does not require any external power source and only utilizes its motions to absorb and dissipate the vibration energy. The most commonly utilized passive control device is the tuned mass damper (TMD), which works by attaching an auxiliary mass to the primary vibrating structure using a spring and a dashpot, as shown in Figure 2-2. The TMD's natural frequency is adjusted to match the vibration frequency of the main structure, causing the damper to resonate out of phase with the structure. This leads to the efficient transfer of vibrational energy from the main structure to the TMD, which is then absorbed and dissipated by the damper. Various implementations of TMD on wind turbines have been proposed, including applying single TMD [12, 13] and bi-directional TMDs [14-16] in the nacelle, installing multiple TMDs in the hollow tower [17], etc.

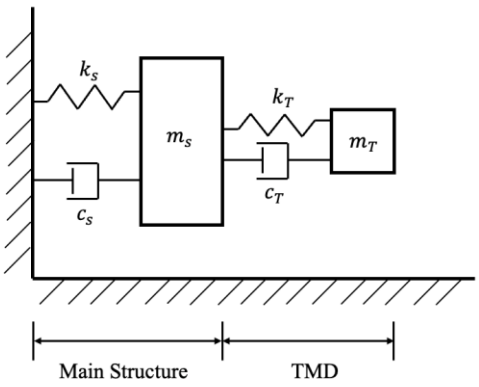

Figure 2-2. A main structure-TMD system [4].

Instead of adopting auxiliary mass as the oscillator to absorb excess energy, liquid has also

been proposed to serve as the energy dissipator. In terms of wind turbine vibration mitigation, tuned liquid column damper (TLCD) [18, 19], tuned liquid column gas damper (TLCGD) [20-22], and tuned liquid damper (TLD) [23-27] have been developed and examined numerically or experimentally. These passive devices are proven effective in suppressing the excessive vibrations on wind turbine towers, by either numerical studies [12, 13, 15, 28, 29] or experimental research [23, 30-32].

However, conventional passive control devices are normally proposed to be installed in the nacelle [12-16, 18-27] and at the upper location inside the tower [17]. In fact, the space in the nacelle is limited due to the existence of other vital parts, such as the gearbox and generator, which makes the installation of vibration control devices not straightforward. Moreover, the space within the tower top is also constrained due to the tower's design, where the radius decreases from bottom to top, posing further limitations on the installation of vibration control devices. Also, to achieve desired vibration mitigation effectiveness, a substantial amount of auxiliary mass is normally required in the conventional passive dampers, which may increase the manufacture and maintenance costs of the wind turbine.

2.3 Development of negative stiffness damper

To minimize the amount of oscillating mass needed to stabilize heavy primary structures, such as high-rise buildings and wind turbine towers, the concept of negative stiffness elements was firstly introduced by Molyneaux [33], and later developed by Platus with milestone progression [34]. The fundamental idea behind negative stiffness elements is to significantly decrease the stiffness of the isolator, which leads to a decrease in the natural frequency of the system to almost zero [35]. This reduction in the natural frequency results in a decrease in the transmissibility of the system for all frequencies above the natural frequency, thus improving the vibration isolation performance.

The primitive negative stiffness oscillators that adopt the mechanism mentioned above are called “Quasi Zero Stiffness” (QZS) oscillators [35]. However, the application of QZS

oscillators leads to a drastic reduction in the stiffness of the structure, which significantly limits the static loading capacity of such structures.

Negative stiffness elements, when combined with positive stiffness components, form the foundation of a range of innovative negative stiffness damper designs. Li et al. [36] thoroughly examined these negative stiffness dampers and presented a comprehensive review. By incorporating negative stiffness elements, the fundamental vibration frequency of the protected structure is effectively reduced, and the force or displacement transmission is minimized, due to the unique behaviour of negative stiffness elements in the system. As depicted by Equation (2) from Li et al. [36], $U = -\frac{1}{2}kD^2$, the potential energy stored within a system subjected to negative stiffness is inversely related to deformation. This negative potential energy indicates a system that loses energy during deformation, characterizing the damping effect of negative stiffness. Furthermore, this damping effect is visually demonstrated in Figure 3, which illustrates the force-displacement relationship in a system exhibiting negative stiffness. The figure shows that at a certain displacement, the force required to maintain the buckled (negative stiffness) state is less than that for the unbuckled state, thus evidencing reduced force transmission. This is essential to understanding how the introduction of negative stiffness elements to a damper design can result in a significant reduction in the transmission of vibrations through the damper, thereby protecting the structure from excessive movements and forces.

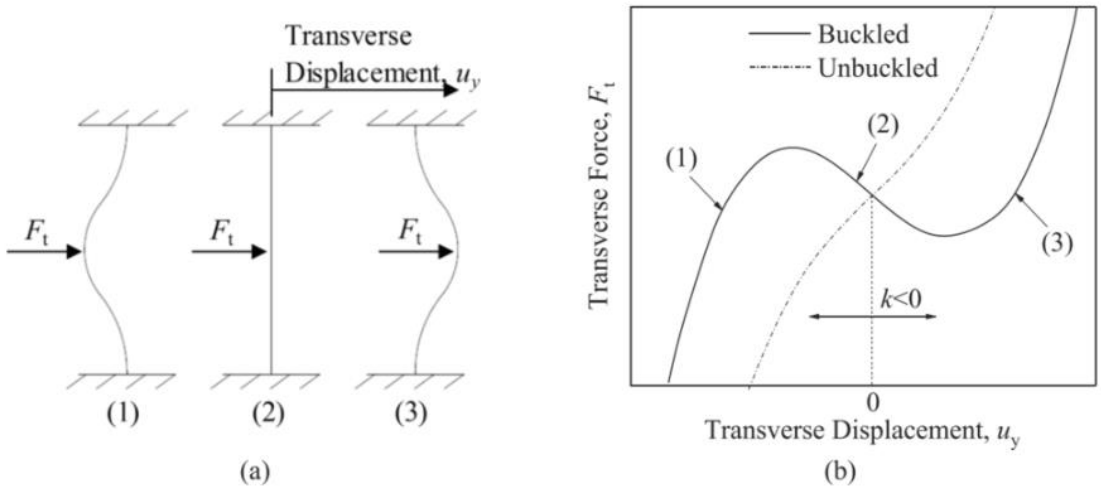

(a) Different transition states (b) Force–displacement relationship

Figure 3. The beam buckling process [36]

Concurrently, positive stiffness elements are employed to provide the necessary load-carrying capacity to the system. This strategic combination allows negative stiffness dampers to achieve a high level of vibration isolation while simultaneously maintaining overall system stability and integrity [36]. Various mechanisms have been reported to realize the negative stiffness elements in the damper such as coil spring [33, 37-39], disk spring [40], pre-bulked beams [41, 42], and magnetism [43]. Several studies have investigated the compatibility and effectiveness of adopting negative stiffness dampers for structural vibration isolation such as in buildings [44-46] and bridges [47-50]. These studies also demonstrated the effectiveness of using negative stiffness dampers for structural vibration isolation.

2.4 KDamper

Based on the 2-DOF negative stiffness oscillator in [51], Antoniadis et al. proposed a novel type of negative stiffness damper dubbed KDamper [52]. An auxiliary mass was added to the internal DOF to achieve some of the vibration mitigation features of TMD. A comparison between the QZS oscillator and the KDamper is provided in Figure 2-4.

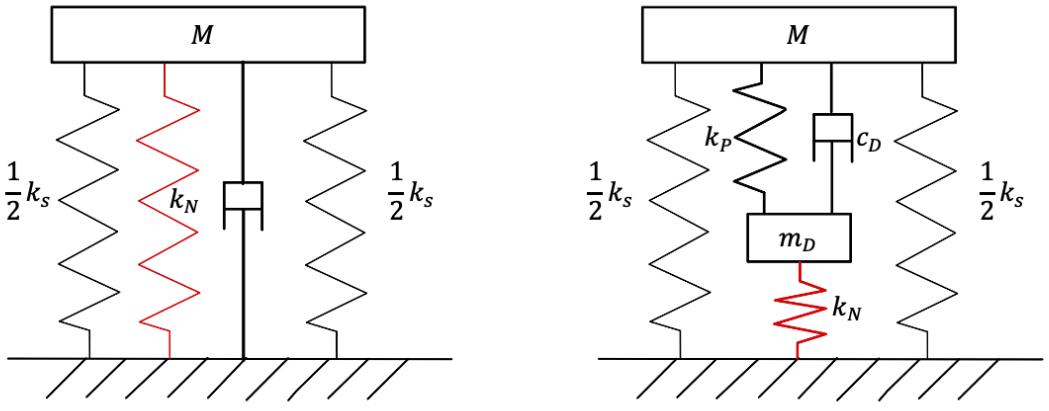

(a) QZS oscillator (b) KDamper

Figure 2-4. Fundamental layout of QZS oscillator and KDamper [52]

The realization of KDamper was then reported by using the horizontal-spring sliders [52] and

disc springs, respectively [53]. Disk spring configuration was also reported to present some extra advantages over horizontal-spring configuration, such as better compactness, abilities to withstand heavy loads and stresses, less mechanical complexity, and improved structural robustness [53]. The outcomes of the analyses indicated its capability to achieve effective vibration mitigation in the entire frequency range with a minimal value of additional mass.

Applications of utilizing KDamper to protect engineering structures, including a single pie bridge [54] and wind turbines [55], from unfavourable vibrations caused by external loadings were recently reported. The numerical results indicated that the utilization of KDamper results in significant reductions in the structural dynamic responses, and usually, the efficacy of the control is more conspicuous as compared to that of conventional vibration mitigation devices (e.g., seismic isolation bearings for the bridge, and TMDs for wind turbines). Although TMDs are known for their straightforward design and robustness, KDamper offers an attractive alternative that upholds acceptable levels of simplicity and reliability but with enhanced damping characteristics that are particularly beneficial in certain challenging applications like wind turbine vibration control.

Figure 2-5 shows the installation layout of KDmaper in the wind turbine as suggested in [55]. As shown, the KDamper was installed at the top of the wind turbine tower, and the negative stiffness element is linked to the ground. The considerable height of the tower may make this design not easy to be implemented in engineering practices.

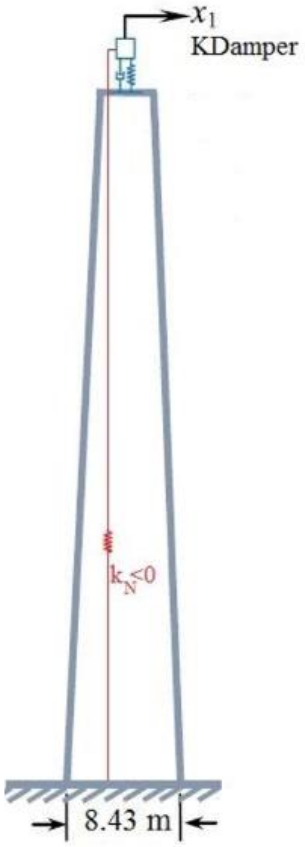

Figure 2-5. The configuration of applying KDamper to a wind turbine model proposed in [55].

2.5 Summary

This chapter presents a comprehensive literature review on the control strategies for wind turbine vibration mitigation, the development of negative stiffness damper, and the concept and application of KDamper are also discussed. The main findings are summarized as follows:

(1) In previous studies, diverse techniques have been suggested to reduce and control the unfavourable vibrations of wind turbines. Conventional passive dampers, such as TMD and TLCD, are normally proposed to be installed at the top of the hollow tower or inside the nacelle to achieve maximum vibration mitigation effectiveness. However, the very limited available space and the requirement of a substantial amount of auxiliary mass make the applications of conventional passive vibration control devices not straightforward.

(2) The integration of negative stiffness elements into vibration control strategies addresses

these limitations by enabling the use of a reduced oscillating mass. This is achieved through the approach of negative stiffness, which allows for the conservation of energy in a manner that requires less mass to be moved by the damper system for effective vibration absorption. By incorporating positive stiffness elements with negative stiffness elements, various designs of negative stiffness dampers were proposed, which made it possible to achieve effective vibration isolation while maintaining system stability.

(3) A novel type of negative stiffness damper, termed KDamper, was proposed and proven to be able to provide superior vibration isolation properties than a TMD. The attempt of adapting KDamper as the vibration control device for wind turbine towers was also reported. However, the proposed installation configuration may make it not easy to be implemented in engineering practice.

Despite the extensive body of work in this area, there remain specific aspects that have not been thoroughly explored and are addressed in this thesis. These include:

(1) Integration and Optimization of KDamper: While existing studies have discussed the concept and potential applications of KDamper, there is a lack of comprehensive research on integrating and optimizing KDamper in wind turbine systems. This thesis contributes by exploring novel ways to implement KDamper, enhancing its efficiency and compatibility with wind turbines.

(2) Comparative Evaluation with Conventional Systems: Prior research has often treated vibration mitigation systems in isolation. This thesis provides a comparative analysis of KDamper with traditional systems like TMD, offering a detailed evaluation of its performance relative to these established technologies.

(3) Addressing Installation and Space Constraints: Although the limited space in wind turbine nacelles for installing vibration control devices is a known issue, there is scarce research on designing dampers that work effectively within these constraints. This thesis aims to address this gap by proposing design modifications for KDamper that make it more suitable for constrained spaces.

(4) Adequacy of Numerical Research on Seismic Excitation: Previous research has not adequately investigated the effectiveness of KDamper under various seismic excitations. This thesis addresses this by optimizing KDamper with white noise to ensure its capability against diverse external excitations. Furthermore, a wide range of earthquake scenarios is chosen to investigate the damper's effectiveness, marking a first in this area of research.

By addressing these research gaps, this thesis aims to make a substantial contribution to the field of wind turbine vibration mitigation, particularly in enhancing the understanding and application of KDamper.

Charpter 3 KDamper and its basic properties

3.1 Basic layout of TMD and KDamper

Figure 3-1(a) shows an undamped main structure (containing a mass M, and stiffness k_S) controlled by a TMD. In a TMD system, the auxiliary mass m_D is linked to the main structure through a spring k_D and a dashpot c_D. By adjusting the natural frequency of the TMD to match that of the main structure, the TMD can vibrate out of phase with the main structure during its vibration, which causes a significant amount of the structural vibration energy to be transferred to the TMD, and this energy is then dissipated by the dashpot. The vibration of the main structure is therefore mitigated.

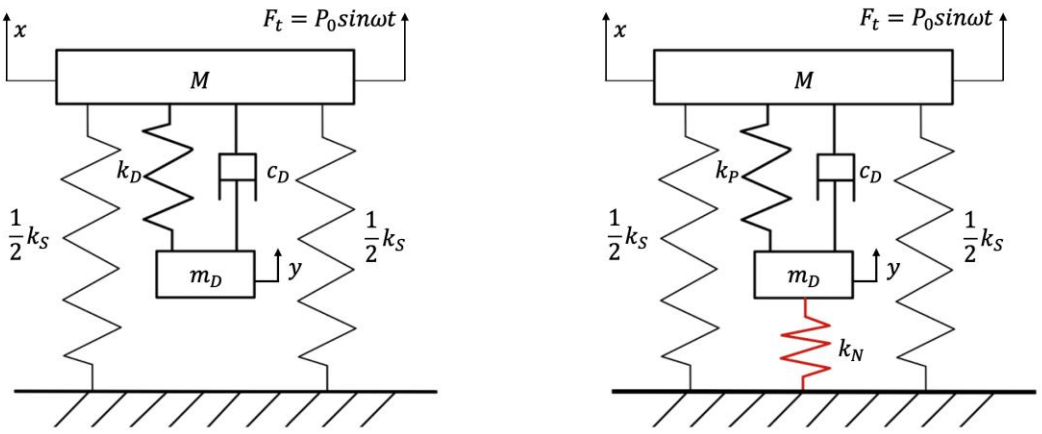

(a) TMD (b) KDamper

Figure 3-1. Fundamental layout of TMD and KDamper

Figure 3-1(b) depicts the configuration of a typical KDamper, which includes a negative stiffness component in its system. Unlike TMD, the additional mass m_D in KDamper is not only linked to the primary structure via a positive stiffness component k_P and a dashpot c_D, but also attached to the foundation through a negative stiffness element possessing a value of k_N. This configuration preserves the system with a total static stiffness as described in Equation (3-1), where k_{st} denotes the total static stiffness of a single-degree-of-freedom (SDoF) system without damping.

$$k_{st} = k_S + \frac{k_P k_N}{k_P + k_N} \tag{3-1}$$

As a result, KDamper overcomes the inherent flaw of QZS oscillators, which are with the very limited loading capacity caused by the drastically decreased static stiffness of the system.

3.2 Optimization and comparison between TMD and KDamper

To compare the performance of KDamper and TMD, and better reveal the basic properties of KDamper, the selection of optimal design parameters is performed for both the TMD and KDamper. To facilitate the optimization of TMD and KDamper, and achieve a clear comparison of the performance between these two types of vibration absorbers, the damping of the main structure is ignored.

As shown in Figure 3-1, an external force with a time-varying value of $F_t = P_0 \sin \omega t$ is applied to the main structure for both the TMD and KDamper systems. The vertical displacement of the main structure, which is the primary component of the system, is denoted by the variable x. Similarly, the vertical displacement of the auxiliary mass is denoted by the variable y. The equation of motion for the TMD system can be expressed as a set of second-order linear differential equations, as shown below:

$$M\ddot{x} + k_S x + k_D(x - y) + c_D(\dot{x} - \dot{y}) = P_0 \sin \omega t \tag{3-2}$$

$$m_D\ddot{y} - k_D(x - y) - c_D(\dot{x} - \dot{y}) = 0 \tag{3-3}$$

Similarly, the equation of motion for the KDamper system is:

$$M\ddot{x} + k_S x + k_P(x - y) + c_D(\dot{x} - \dot{y}) = P_0 sin\omega t \tag{3-4}$$

$$m_D\ddot{y} - k_P(x - y) + k_N y - c_D(\dot{x} - \dot{y}) = 0 \tag{3-5}$$

Equations (3-2) and (3-3) can be expressed in the frequency domain as follows:

$$-\omega^2 MX + k_S X + k_D(X - Y) + j\omega c_D(X - Y) = P_0 \tag{3-6}$$

$$-\omega^2 m_D Y - k_D(X-Y) - j\omega c_D(X-Y) = 0 \tag{3-7}$$

and the equations of motion of the KDamper system become:

$$-\omega^2 MX + k_S X + k_P(X-Y) + j\omega c_D(X-Y) = P_0 \tag{3-8}$$

$$-\omega^2 m_D Y - k_P(X-Y) + k_N Y - j\omega c_D(X-Y) = 0 \tag{3-9}$$

where X and Y are the complex response amplitudes, as in:

$$x(t) = X\exp(j\omega t) \tag{3-10}$$

$$y(t) = Y\exp(j\omega t) \tag{3-11}$$

It is apparent that the equations of motion for the TMD system and the KDamper system are identical when the negative stiffness element terms ($k_N y$, $k_N Y$) are not present. From the complex form of motion equation sets, the transfer function of both systems can be derived:

For TMD:

$$\frac{X}{x_{st}} = \frac{[(-\omega^2 m_D + k_D) + j\omega c_D]k_S}{[(-\omega^2 M + k_S)(k_D - \omega^2 m_D) - \omega^2 m_D k_D] + j\omega c_D(-\omega^2 m_D - \omega^2 M + k_S)} \tag{3-12}$$

where x_{st} is the static deflection of the main structure in Figure 3-1(a), which is given by:

$$x_{st} = P_0/k_S \tag{3-13}$$

For KDamper:

$$\frac{X}{x_{st}} = \frac{[(-\omega^2 m_D + k_P + k_N) + j\omega c_D]k_S}{(-\omega^2 M + k_S + k_P + j\omega c_D)(-\omega^2 m_D + k_P + k_N + j\omega c_D) - (k_P + j\omega c_D)^2} \tag{3-14}$$

where x_{st} is the static deflection of the main structure in Figure 3-1(b), which is given by:

$$x_{st} = P_0 / \left(k_S + \frac{k_P \cdot k_N}{k_P + k_N} \right) \tag{3-15}$$

From which the expressions of transmissibility (T_r) can be derived by eliminating the imaginary terms in the transfer functions:

For TMD:

$$T_r = \left| \frac{X}{x_{st}} \right| = \sqrt{\frac{[(-\omega^2 m_D + k_D) + (\omega c_D)^2]\, {k_S}^2}{[(-\omega^2 M + k_S)(k_D - \omega^2 m_D) - \omega^2 m_D k_D]^2 + (\omega c_D)^2 (-\omega^2 m_D - \omega^2 M + k_S)^2}} \tag{3-16}$$

For KDamper:

$$T_r = \left| \frac{X}{x_{st}} \right| = \sqrt{\frac{[(-\omega^2 m_D + k_P + k_N) + (\omega c_D)^2]\, {k_S}^2}{[(-\omega^2 M + k_S + k_P)(k_D - \omega^2 m_D) - k_P^2]^2 + (\omega c_D)^2 [(-\omega^2 M + k_S + k_P)(k_D - \omega^2 m_D) - 2k_P]^2}} \tag{3-17}$$

To get the dimensionless form of the transmissibility, the following parameters are defined:

Natural Frequency of the System: $\omega_n = \sqrt{k_S / M}$ (3-18)

Natural Frequency of the TMD: $\omega_D = \sqrt{k_D / m_D}$ (3-19)

Natural Frequency of the KDamper: $\omega_D = \sqrt{(k_P + k_N) / m_D}$ (3-20)

Damping Ratio of the TMD: $\xi_D = c_D / 2\sqrt{m_D k_D}$ (3-21)

Damping Ratio of the KDamper: $\xi_D = c_D / 2\sqrt{m_D (k_P + k_N)}$ (3-22)

Mass Ratio: $\mu = m_D / M$ (3-23)

Natural Frequency Ratio: $f = \omega_D / \omega_n$ (3-24)

Forced Frequency Ratio: $g = \omega / \omega_n$ (3-25)

Negative Stiffness Ratio: $R_k = -k_N / k_D = -k_N / (k_N + k_P)$ (3-26)

Then, for both systems, the dimensionless form of transmissibility can be expressed as:

$$T_r = \sqrt{\frac{A^2 + (2\xi_D)^2 B^2}{C^2 + (2\xi_D)^2 D^2}} \tag{3-27}$$

where, for TMD:

$$A = f^2 - g^2 \tag{3-28}$$

$$B = f \cdot g \tag{3-29}$$

$$C = g^4 - g^2(1 + \mu f^2 + f^2) + f^2 \tag{3-30}$$

$$D = gf[1 - g^2(1 + \mu)] \tag{3-31}$$

and, for KDamper:

$$A = f^2 - g^2 \tag{3-32}$$

$$B = f \cdot g \tag{3-33}$$

$$C = g^4 - g^2[1 + \mu f^2(1 + R_k)^2 + f^2] + f^2 \tag{3-34}$$

$$D = gf[1 - g^2(1 + \mu) + \mu f^2 R_k^2] \tag{3-35}$$

It can be noticed that if the negative stiffness ratio is set to zero, i.e., $R_k = 0$, Equation (3-34) will be reduced to Equation (3-30), and Equation (3-35) will be reduced to Equation (3-31). With the dimensionless expression of transmissibility, the optimal natural frequency ratio (f_{opt}) can be found out by satisfying the following equation:

$$\frac{\partial T_r}{\partial \xi_D} = 0 \tag{3-36}$$

which yields:

For TMD:

$$f_{opt} = \frac{1}{1+\mu} \tag{3-37}$$

For KDamper:

$$f_{opt} = \sqrt{\frac{1}{(1+\mu)(1+\mu+\mu R_k) - \mu R_k^2}} \tag{3-38}$$

Due to the intricate and lengthy nature of the derivation process, the full set of steps to obtain the optimal natural frequency ratio from Equation (3-36) for the KDamper is beyond the scope of this document. Reference [52] should be consulted for the detailed derivation.

From which, the expression of the optimal maximum transmissibility ($T_{r\max\,(opt)}$) of the two systems are:

For TMD:

$$T_{r_{max\,(opt)}} = \sqrt{\frac{\mu+2}{\mu}} \tag{3-39}$$

For KDamper:

$$T_{r_{max\,(opt)}} = \sqrt{\frac{\mu+2}{\mu}} \cdot \left[\frac{(1+\mu+\mu R_k)(1+\mu) - \mu R_k^2}{(1+\mu)^2(1+R_k)}\right] \tag{3-40}$$

The optimal selection of the damping ratio for TMD can be derived from Equation (3-36):

$$\xi_{D\_opt} = \sqrt{3\mu/8(1+\mu)^3} \tag{3-41}$$

While the analytical determination of the optimal damping ratio for the KDamper presents complexities, a numerical search method is typically employed to pinpoint its value. In this approach, the objective function is defined as minimizing the maximum value of the transfer function. This involves identifying the damping ratio at which the transfer function's maximum value reaches its lowest point. The search is constrained within the physically

meaningful range of the damping ratio, specifically between 0 and 1. As the search progresses and approaches the optimal value, the step size of the numerical search is decreased to achieve the desired value with a certain level of precision. By iteratively adjusting the damping ratio within this range and evaluating its impact on the objective function, the optimal value that offers the best performance for the KDamper system can be identified. This numerical method provides a practical and efficient means to optimize the system in scenarios where analytical solutions might be elusive.

3.3 Basic properties of KDamper

The results of optimal parameters selection lead to three basic properties of KDamper:

Property 1: Under a given mass ratio μ, KDamper always provides a better vibration mitigation effect compared to TMD.

Figure 3-2 shows the optimized transmissibility curves of KDamper with a specified mass ratio ($\mu = 1/20$) for different negative stiffness ratio values ($R_k = 0,\ 0.5,\ 1,\ 1.5$). The black curve corresponds to zero negative stiffness, under which the KDamper system is reduced to the TMD system. A significant reduction of the peak values of the optimal transmissibility is observed when coloured lines (KDamper, $R_k \neq 0$) are compared with the black line (TMD, $R_k = 0$), which verifies the statement of property 1.

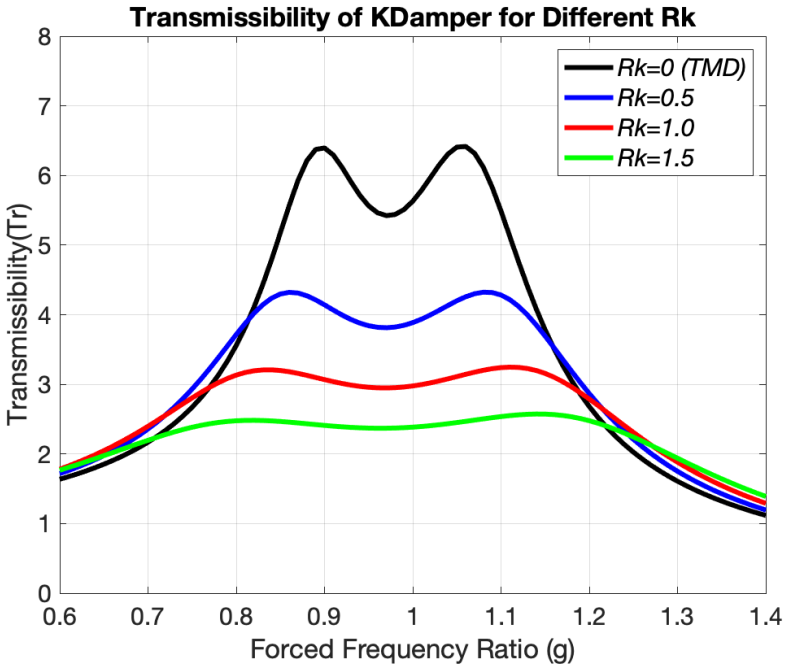

Figure 3-2. Transmissibility of KDamper for different negative stiffness ratios.

Property 1 can also be proved through analytical analysis:

Dividing Equation (3-40) by Equation (3-39), and define the ratio between the optimal maximum transmissibility of KDamper and TMD as τ:

$$\tau = \frac{T_{r\max(opt)}(KD)}{T_{r\max(opt)}(TMD)} = \frac{(1+\mu+\mu R_k)(1+\mu)-\mu R_k^2}{(1+\mu)^2(1+R_k)} \tag{3-42}$$

Subtracting the numerator from the denominator in Equation (3-42) results in the following equation:

$$\begin{aligned}(1+\mu)^2(1+R_k)-(1+\mu+\mu R_k)(1+\mu)-\mu R_k^2 \\ = R_k\cdot(1+\mu+\mu R_k)\geq 0\end{aligned} \tag{3-43}$$

The relation in Equation (3-43) clearly implies that $\tau \leq 1$. Thus, the optimal maximum transmissibility of KDamper is always smaller than that of TMD ($T_{r\max(opt)}(KD) \leq T_{r\max(opt)}(TMD)$).

Property 2: The effectiveness of vibration isolation in KDamper can be improved by increasing the negative stiffness element's absolute value instead of increasing the auxiliary

mass (μ).

For a properly tunned TMD system, the only way to achieve a better vibration isolation effect is by increasing the weight of the auxiliary mass, which will inevitably cause higher manufacturing and maintenance costs, as well as lower structural stability, especially for high-rise structures. However, KDamper can provide better vibration mitigation by increasing the negative stiffness ratio (R_k). As shown in Figure 3-2 and Figure 3-3, the increase in the negative stiffness ratio leads to a drastic reduction not only in maximum transmissibility but also in the average value of transmissibility over a wide range of external excitation frequency.

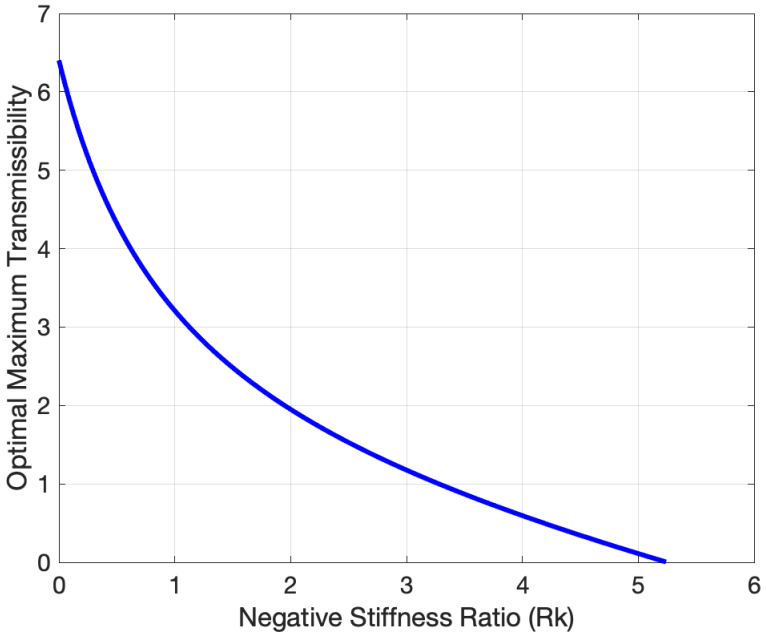

Figure 3-3. Optimal maximum transmissibility versus negative stiffness ratio.

Property 3: The increment of the negative stiffness element (R_k) in KDamper should be within the upper limit of the static stability of the structure. The static stability limit is defined as the maximum value of the negative stiffness element (R_k), which ensures that the entire system remains stable and does not collapse due to negative stiffness. Therefore, the magnitude of R_k should be carefully selected and evaluated to avoid compromising the stability and safety of the structure.

Equating the denominator of Equation (3-38) to zero gives:

$$(1+\mu)(1+\mu+\mu R_k) - \mu R_k^2 = 0 \tag{3-44}$$

The solution to Equation (3-44) provides the maximum negative stiffness ratio (R_{k_max}) that can be incorporated into the KDamper system before compromising the static stability limit of the structure:

$$R_{k\_max} = (1+\mu) \cdot \frac{1+\sqrt{1+4/\mu}}{2} \tag{3-45}$$

However, in practice, the selection of a negative stiffness element should take not only Equation (3-1) and Equation (3-45) into consideration. In fact, negative stiffness designs may exhibit complex, nonlinear behaviours that can affect the stability and performance of the overall structure. These behaviours often arise from the inherent instability of nonlinear systems, which may lead to unexpected oscillations and instabilities. Therefore, when incorporating a negative stiffness element into a structure, it is crucial to consider and account for such nonlinearities to ensure the stability and safety of the system. Moreover, other factors, such as temperature variations, external loads, and material degradation, can also affect the performance of the negative stiffness element and the overall system, and thus should be carefully considered during the design and implementation stages.

Chapter 3 presents a comprehensive analysis and optimization of vibration damping strategies, with a significant portion of the theoretical foundation and analytical formulas directly sourced from [52]. While the development of these analytical expressions and the foundational concepts underlying them are attributed to the work presented in [52], this thesis extends upon that groundwork through additional numerical analysis and coding efforts, particularly in determining the damping ratio and its implications in practical applications. It is important to clarify that the original development of these formulas is not the contribution of this thesis but rather the utilization and application of these established principles to specific scenarios and extended numerical analyses are the focus of this study.

Charpter 4 Analytical model and optimal design of KDamper

4.1 Properties of the NREL 5 MW wind turbine model

The three-blade wind turbine from the National Renewable Energy Laboratory (NREL) report [55] is selected as the model wind turbine in the present study as its properties are well defined in the report and it is investigated in many previous studies [2]. The selected wind turbine possesses a rated capacity of 5 MW, featuring a rotor diameter of 126 m and a tower height of 87.6 m. The comprehensive properties associated with the NREL 5 MW wind turbine have been acquired from the report and are systematically presented in Table 4-1.

Table 4-1. Gross properties of NREL 5MW wind turbine

Tower Height (m)	87.6
Tower Base/Top Diameter (m)	6/3.87
Tower Base/Top Thickness (m)	0.0351/0.0247
Tower Adjusted Mass Density (kg/m^3)	8500
Young's Modulus (GPa)	210
Rotor Mass (kg)	110,000
Nacelle Mass (kg)	240,000

From the geometry and mechanical properties in Table 4-1, the distributed properties of the tower are calculated and listed in Table 4-2.

Table 4-2. Distributed tower properties

Elevation (m)	Height Fraction	Mass Density (kg/m)	Flexural Rigidity (N*m^2)	Inertia Density (kg*m)
0.00	0.0	5590.87	614.34E+9	24865.3
8.76	0.1	5232.42	534.82E+9	21646.7
17.52	0.2	4885.76	463.27E+9	18750.6
26.28	0.3	4550.87	399.13E+9	16154.7
35.04	0.4	4227.75	341.88E+9	13837.6
43.80	0.5	3916.40	291.01E+9	11778.6
52.56	0.6	3616.83	246.03E+9	9957.8
61.32	0.7	3329.03	206.46E+9	8356.3
70.08	0.8	3053.01	171.85E+9	6955.6

78.84	0.9	2788.75	141.78E+9	5738.3
87.60	1.0	2536.27	115.82E+9	4687.7

4.2 Model development

4.2.1 Assumptions

The rotor's geometry can have a considerable impact on the vibration characteristics of a wind turbine, particularly when it is in operation. This is due to the periodic change in blade positions and the centrifugal stiffness produced by the rotating blades, which in turn enhances the stiffness and natural frequencies of the blades [56]. Murtagh et al. [56] further noted that while blade rotation primarily affects the vibration characteristics of the blades themselves, its influence on the tower is comparatively less significant. In this study, the focus is on examining the efficacy of using KDamper to mitigate the tower vibration of wind turbines under parked condition. As a result, the geometries of the nacelle and blades are considered to have a negligible impact. The analytical model only takes into account the masses of the nacelle and blades, which are represented by a lumped mass element situated at the top of the tower, without considering the blades' moment of inertia.

4.2.2 Lumped mass simplification

The equation of motion of the 5MW wind turbine model is expressed as:

$$\boldsymbol{m\ddot{u} + c\dot{u} + ku = -mI\ddot{x}_g} \tag{4-1}$$

where $\boldsymbol{m}$, $\boldsymbol{k}$ and $\boldsymbol{c}$ are the inertia matrix, lateral stiffness matrix and damping matrix, respectively.

To acquire the structural dynamic characteristics of the NREL 5MW wind turbine, alongside the assumption made above, the masses of the tower, rotor and nacelle are distributed into 10 mass points as shown in Figure 4-1. These 10 mass points are located on the cross points of the central line of the tower and the cross sections corresponding to the height fractions from 0.1 to 1.0. The mass of each mass point is estimated from the cross-sectional mass density

provided in Table 4-2:

For $n = 1{\sim}9$: $$m_n = md_n \cdot L \tag{4-2}$$

For $n = 10$: $$m_{10} = \left(\frac{1}{2}\right) L \cdot md_n + m_{NR} \tag{4-3}$$

where md_n is the cross-sectional mass density; L is the segment length and $L = 8.76m$ based on Table 4-2; and m_{NR} is the mass of the rotor and nacelle, which is $m_{NR} = 350{,}000kg$.

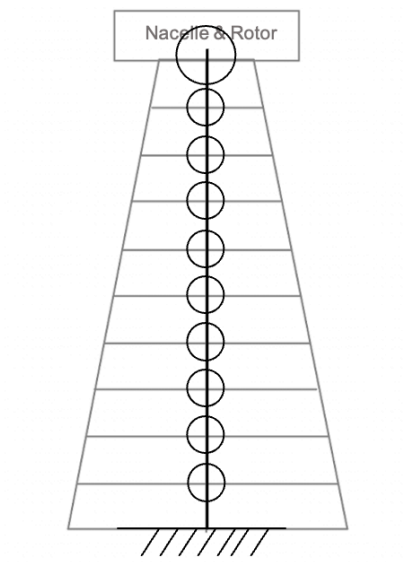

Figure 4-1. Lumped mass simplification

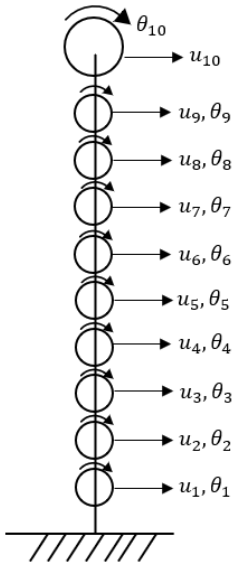

Figure 4-2. DoFs of lumped mass model

Considering each mass point has two degrees of freedom (DoFs): one for the transverse movement, denoted as u_n, and the other for the rotational movement, denoted as θ_n, as shown in Figure 4-2, the moment of inertia of each cross section is calculated as below:

For $n = 1{\sim}9$: $$I_n = Id_n \cdot L \tag{4-4}$$

For $n = 10$: $$I_{10} = \left(\frac{1}{2}\right) L \cdot Id_n \tag{4-5}$$

where I_n is the moment of inertia of the nth mass point, and Id_n is the corresponding inertia density given in Table 4-2. According to the definition of inertia influence coefficient given

in many textbooks related to structural dynamics (e.g., [57]), the inertia matrix of the lumped mass model can be assembled as below:

$$[m] = \begin{bmatrix} m_1 & & & & \\ & I_1 & & 0 & \\ & & \ddots & & \\ & 0 & & m_{10} & \\ & & & & I_{10} \end{bmatrix}_{20\times 20} \tag{4-6}$$

For each segment with a mass point at its ends, the elemental lateral stiffness is as below:

$$[k_n] = \begin{bmatrix} A_n & B_n \\ C_n & D_n \end{bmatrix}_{4\times 4} \tag{4-7}$$

where,

$$[A_n] = \begin{bmatrix} \frac{12 \cdot EI_n}{L^3} & \frac{6 \cdot EI_n}{L^2} \\ \frac{6 \cdot EI_n}{L^2} & \frac{4 \cdot EI_n}{L} \end{bmatrix} \tag{4-8}$$

$$[B_n] = \begin{bmatrix} -\frac{12 \cdot EI_n}{L^3} & \frac{6 \cdot EI_n}{L^2} \\ -\frac{6 \cdot EI_n}{L^2} & \frac{2 \cdot EI_n}{L} \end{bmatrix} \tag{4-9}$$

$$[C_n] = \begin{bmatrix} -\frac{12 \cdot EI_n}{L^3} & -\frac{6 \cdot EI_n}{L^2} \\ \frac{6 \cdot EI_n}{L^2} & \frac{2 \cdot EI_n}{L} \end{bmatrix} \tag{4-10}$$

$$[D_n] = \begin{bmatrix} \frac{12 \cdot EI_n}{L^3} & -\frac{6 \cdot EI_n}{L^2} \\ -\frac{6 \cdot EI_n}{L^2} & \frac{4 \cdot EI_n}{L} \end{bmatrix} \tag{4-11}$$

in which EI_n is the flexural rigidity given in Table 4-2. To obtain the global lateral stiffness matrix of the lumped mass model, these 10 elemental lateral stiffness matrices need to be assembled with the stiffness coefficients of common nodes being added together, as shown below:

$$[k] = \begin{bmatrix} D_1 + A_2 & B_2 & & & 0 \\ C_2 & D_2 + A_3 & B_3 & & \\ & C_3 & \ddots & \ddots & \\ & & \ddots & D_9 + A_{10} & B_{10} \\ 0 & & & C_{10} & D_{10} \end{bmatrix}_{20\times 20} \tag{4-12}$$

The natural frequencies and mode shapes of a system can be found by solving the eigenvalue problem using the system's mass matrix and lateral stiffness matrix:

$$[\Phi, \Omega^2] = eig\left(\frac{[k]}{[m]}\right) \tag{4-13}$$

where Φ is the modal matrix and Ω^2 is the spectral matrix of the eigenvalue problem:

$$[\Omega^2] = \begin{bmatrix} \omega_1^2 & & & \\ & \omega_2^2 & & \\ & & \ddots & \\ & & & \omega_{20}^2 \end{bmatrix}_{20\times 20} \tag{4-14}$$

where $\omega_1 \ldots \omega_{20}$ are the natural frequencies of the lumped mass model sequenced from the smallest to the largest. The obtained first two natural frequencies are compared with the values provided by the NREL report [55], and with the value given by the finite element model developed in ABAQUS [17], as shown in Table 4-3. It can be seen that the errors between the three sets of data are within 3%, which is acceptable. The first two normalized mode shapes are shown in Figure 4-3, which are consistent with the reported results as well.

Table 4-3. Result comparisons on the natural frequencies of the wind turbine tower

	Present study	NREL report	FE model
1st Natural Frequency (Hz)	0.3357	0.3240	0.3263
2nd Natural Frequency (Hz)	3.0585	2.9003	2.9566

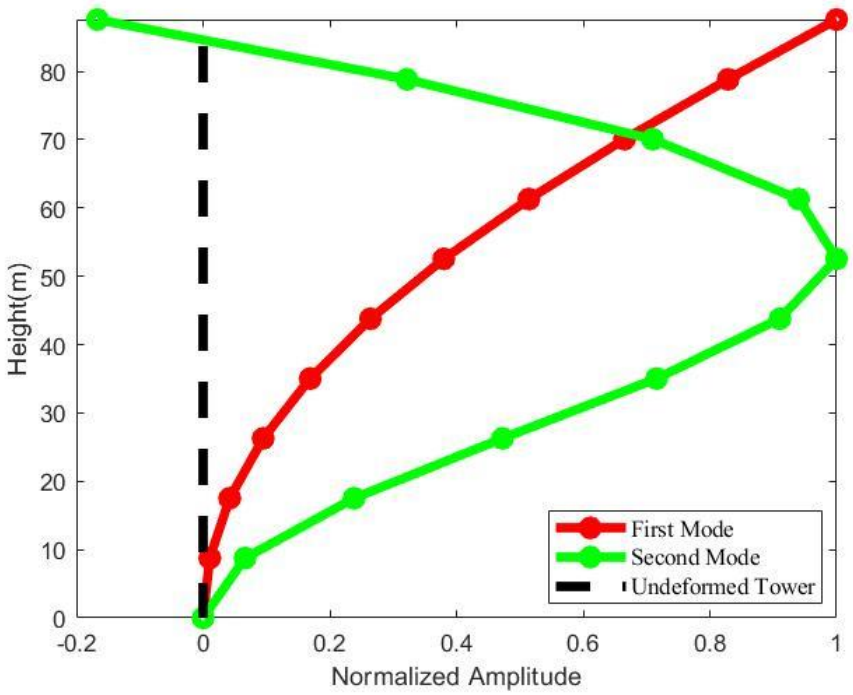

Figure 4-3. Normalized mode shapes

The responses of the tower are predominantly determined by its first two vibration modes. As illustrated in Figure 4-3, the first mode shape displays its maximum amplitude at the top of the tower, while the second mode shape exhibits its peak amplitude at a point situated approximately 40 meters below the top of the tower.

Wind turbine damping mechanisms are complex, typically involving aerodynamic damping, structural damping, and soil damping. These distinct types of damping account for the contributions from wind, tower structure, and supporting soil to the overall damping behaviour of the system [58]. Koukoura et al. [59] carried out experimental studies to ascertain the damping ratio of a wind turbine at a standstill conidtion, determining a value of 1.93%. Katsanos et al. [60] noted that the damping ratio for a parked wind turbine generally ranges from 0.5% to 2%. To simplify the modelling process, the tower's damping is represented by the Rayleigh damping approach, adopting a 2% damping ratio for the first two vibration modes [57]:

$$[c] = a_0[m] + a_1[k] \tag{4-15}$$

where:

$$a_0 = \xi \frac{2\omega_1\omega_2}{\omega_1 + \omega_2} \tag{4-16}$$

$$a_1 = \xi \frac{2}{\omega_1 + \omega_2} \tag{4-17}$$

The three matrices of the simplified wind turbine model, namely inertia, damping and lateral stiffness matrix, all have a size of 20 by 20, as the lumped mass model has 20 degrees of freedom.

4.3 Damper application

The configurations of applying a KDamper and a TMD to a wind turbine tower to control its excessive vibration have been explored in [55]. However, as discussed in Chapter 2, connecting the additional mass of KDamper from the tower top to the ground with a negative stiffness element, as shown in Figure 2-5, is not easy to achieve in engineering practices, due to the height of the wind turbine tower.

In this research, as shown in Figure 4-4, the auxiliary masses of both the KDamper and TMD are connected to the top mass point (m_{10}) using a positive stiffness spring (k_P) and a dashpot (c_D), while for KDamper, the auxiliary mass is also connected to the mass points below the tower top ($m_9, m_8 \ldots m_1$) and the ground respectively, as shown in Figure 4-4(b), to find out the optimal configuration of the KDamper. In the numerical analysis, the assumption is made that external excitations act exclusively in the fore-aft orientation of the tower (x direction, as depicted in Figure 4-4). Consequently, the control devices are incorporated solely in the x direction. This simplification allows for a more focused examination of the tower's response to excitations in the primary direction of interest, while still providing valuable insights into the system's dynamic behavior and the effectiveness of the control devices.

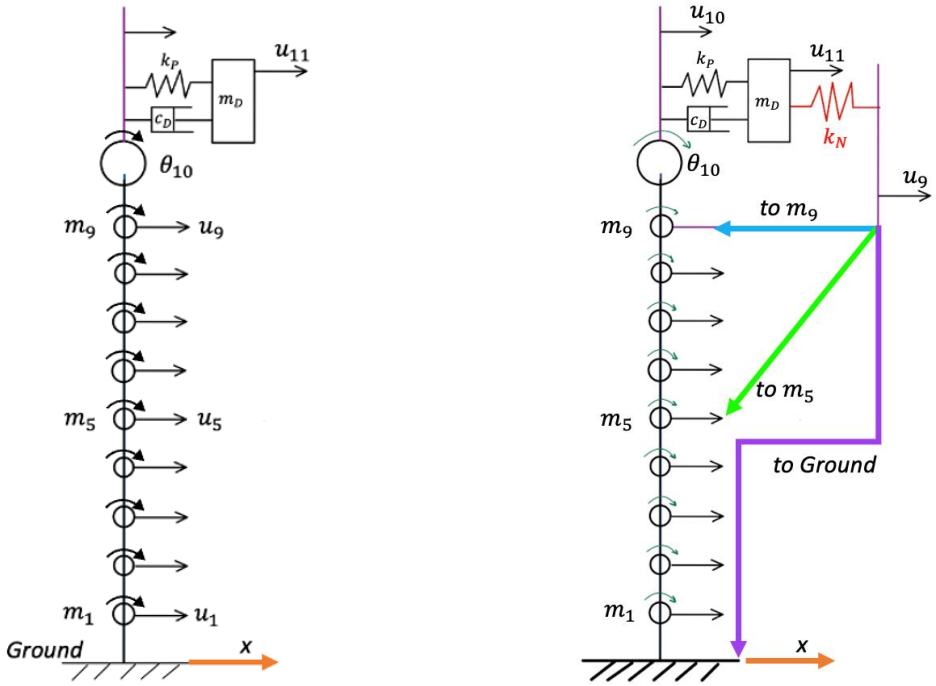

(a) TMD (b) KDamper

Figure 4-4. Schematics of applying different dampers to the lumped mass model

The inertia, damping and lateral matrices of the uncontrolled system are already obtained. However, after the implementation of TMD and KDamper, these three matrices should be modified. The modification process is the same for TMD and KDamper, for the reason that TMD can be obtained when the negative stiffness element in the KDamper is set to zero. The following summarises the modifications:

When the negative stiffness element is connected to the mass points $m_1 \sim m_9$, the modified inertia matrix $[m_D]$ is given by:

$$[m_D] = \begin{bmatrix} [m]_{20\times20} & [0]_{20\times1} \\ [0]_{1\times20} & m_D \end{bmatrix}_{21\times21} \tag{4-18}$$

in which, $[m]_{20\times20}$ is the mass matrix of the naked wind turbine system as represented by Eq. (4-5).

The modified damping matrix $[c_D]$ is given by:

$$[c_D] = \begin{bmatrix} [c]_{20\times20} & [0]_{20\times1} \\ [0]_{1\times20} & 0 \end{bmatrix}_{21\times21} + \begin{bmatrix} [0]_{18\times18} & [0]_{18\times3} \\ [0]_{3\times18} & [c_M] \end{bmatrix}_{21\times21} \tag{4-19}$$

where $[c]_{20\times20}$ is represented by Eq. (4-14); $[c_M]$ is the damping modification matrix, and it has the following form:

$$[c_M] = \begin{bmatrix} c_D & 0 & -c_D \\ 0 & 0 & 0 \\ -c_D & 0 & c_D \end{bmatrix}_{3\times3} \tag{4-20}$$

For the modified lateral stiffness matrix $[k_D]$, when the negative stiffness element is connected to the nth mass point ($n = 1\sim9$), $[k_D]$ is given by:

$$\begin{aligned}[k_D] = &\begin{bmatrix} [k]_{20\times20} & [0]_{20\times1} \\ [0]_{1\times20} & 0 \end{bmatrix}_{21\times21} + \begin{bmatrix} [0]_{18\times18} & [0]_{18\times3} \\ [0]_{3\times18} & [k_{M1}] \end{bmatrix}_{21\times21} \\ &+ \begin{bmatrix} [0]_{2(n-1)\times2(n-1)} & [0]_{2(n-1)\times(23-2n)} \\ [0]_{(23-2n)\times2(n-1)} & [k_{M2}] \end{bmatrix}_{21\times21}\end{aligned} \tag{4-21}$$

where $[k]_{20\times20}$ is represented by Eq. (4-11), and $[k_{M1}]$ and $[k_{M2}]$ are the stiffness modification matrix, given by:

$$[k_{M1}] = \begin{bmatrix} k_P & 0 & -k_P \\ 0 & 0 & 0 \\ -k_P & 0 & k_P + k_N \end{bmatrix}_{3\times3} \tag{4-22}$$

$$[k_{M2}] = \begin{bmatrix} k_N & [0]_{1\times(21-2n)} & -k_N \\ [0]_{(21-2n)\times1} & & \\ -k_N & & [0]_{(22-2n)\times(22-2n)} \end{bmatrix}_{(23-2n)\times(23-2n)} \tag{4-23}$$

When the negative stiffness element is connected to the ground, the modified inertia and damping matrices are also given by Equations (4-18) and (4-19), respectively, while the modified lateral stiffness matrix is:

$$[k_D] = \begin{bmatrix} [k]_{20\times20} & [0]_{20\times1} \\ [0]_{1\times20} & 0 \end{bmatrix}_{21\times21} + \begin{bmatrix} [0]_{18\times18} & [0]_{18\times3} \\ [0]_{3\times18} & [k_{M1}] \end{bmatrix}_{21\times21} \tag{4-24}$$

The modified inertia $[m_D]$, damping $[c_D]$ and lateral stiffness $[k_D]$ matrix all have a size of

21 by 21 as an additional degree of freedom has been introduced by the transverse movement of the auxiliary mass m_D. With the above matrices, the dynamic responses of the wind turbine with a control device can be conveniently calculated by solving the dynamic equation of motion.

To examine the efficacy of KDamper in reducing vibrations and to determine the optimal configuration for implementing KDamper within the wind turbine model, the current study examines the following three scenarios:

1. Uncontrolled wind turbine tower.
2. With a single TMD placed at the top of the tower. A fixed mass ratio $\mu = 2\%$ will be considered. This selection is based on its prevalence in existing research, where a 2% mass ratio has been commonly utilized for TMD systems in wind turbine applications. This choice facilitates a more direct and meaningful comparison between the performance of the KDamper and traditional TMD systems. The values of absorber damping ratio (ξ_D) and positive stiffness element (k_P) will be determined in the parameters optimization section below.
3. With a KDamper installed at the tower top, and the negative stiffness element being connected to different mass points. KDamper shares the same mass ratio as the TMD setup, other parameters including positive stiffness element (k_P), negative stiffness element (k_N) and absorber damping ratio (ξ_D) will be determined in Section 4.4.

4.4 Parameter optimization

Since the groundbreaking work of Den Hartog [61], a multitude of methods have been proposed by various researchers (e.g. [62-71]) to determine the optimal parameters for a TMD. In an attempt to reveal the maximum potential vibration mitigation performances of TMD and KDamper, and perform an intuitive comparison between the performances of the two types of damper, the following parameters need to be defined or optimally selected:

1. Mass Ratio ($\mu = m_D/M$): For both TMD and KDamper, increasing the mass ratio always brings better vibration mitigation effectiveness. Thus, in this research, the mass ratio is set to 2%, which is a typical choice in many engineering practices.
2. Negative Stiffness Ratio ($R_k = -k_N/k_D = -k_N/(k_N + k_P)$): As discussed in section 2, similar to mass ratio, a higher value of negative stiffness ratio provides better vibration isolation performance. However, its value should be constrained based on structure stability and manufacturing restrictions [72]. To better explore the influence of negative stiffness ratio on a damped system with multiple degrees of freedom, three values are assigned to R_k ($R_k = 0.5, 1, 1.5$). The system is optimised based on these three values of R_k respectively.
3. Natural Frequency Ratio ($f = \omega_D/\omega_n$): The optimal natural frequency ratio (f_{opt}) is selected based on the numerical searching method. In determining the optimal natural frequency ratio (f_{opt}) using numerical methods, a search range of 0.1 to 2 is set. This range is chosen because 0.1 accounts for dampers mitigating low-frequency vibrations, while 2 caters to those addressing higher-frequency vibrations. For precise identification within this range, the search progresses in increments of 0.001. Once f_{opt} is determined, the stiffness of the spring element (k_N, k_P) of TMD and KDamper is also determined.
4. Damping Ratio of the Oscillator ($\xi_D = c_D/2\sqrt{m_D k_D}$): The damping ratio is another critical parameter that plays an important role in determining the effectiveness of both the TMD and KDamper systems. For its optimization, a numerical research searching method is employed, with the range set between 0 and 1. This range is chosen because a damping ratio less than 0 is not physically meaningful, and values greater than 1 indicate an overdamped system, which may not be ideal for vibration mitigation. To ensure precision, the search progresses in increments of 0.001. The selection of an optimal damping ratio (ξ_{D_opt}) is accomplished through numerical searching method in conjunction with the selection of the optimal natural frequency ratio f_{opt}.

As depicted in Table 4-3, the natural frequencies of the vibration modes of the wind turbine model under investigation are well-spaced from one another. Given that the objective of the control effort is to minimize the mean square displacement of the tower top, all parameters are optimized exclusively with respect to the first vibration mode. To identify the optimal parameters that offer the most effective vibration mitigation for the wind turbine tower under various external excitations, which consist of a broad spectrum of frequency components, the optimization process is carried out by minimizing the transmissibility of the Multi-Degree-of-Freedom (MDoF) system as developed in Section 4.3 Damper application.

The dynamic behaviour of the uncontrolled and controlled systems can be described in the frequency domain by:

$$\boldsymbol{X}(\omega) = \boldsymbol{H}(\omega)\boldsymbol{P}(\omega) \tag{4-25}$$

where:

$\boldsymbol{X}(\omega)$ is the tower response in the frequency domain; (4-26)

$\boldsymbol{H}(\omega)$ is the transfer function defined by [73]:

$$\boldsymbol{H}(\omega) = [\boldsymbol{K} - \boldsymbol{M}\omega^2 + i\boldsymbol{C}\omega]^{-1} \tag{4-27}$$

$\boldsymbol{P}(\omega)$ is the external excitation in the frequency domain, and

$$\boldsymbol{P}(\omega) = -\boldsymbol{M}\boldsymbol{I}\ddot{x}_g(\omega) \tag{4-28}$$

The power spectral density (PSD) of the excitation ($\boldsymbol{S_{pp}}$) is given by [73]:

$$\boldsymbol{S_{pp}} = \boldsymbol{M}\boldsymbol{I}\boldsymbol{I}^{\boldsymbol{T}}\boldsymbol{M}^{\boldsymbol{T}}S_{\ddot{x}_g} \tag{4-29}$$

In this equation, $\boldsymbol{I}$ represents the influence coefficient matrix. This matrix is structured such that its elements are assigned the value of 1 when the corresponding degrees of freedom (DoFs) are aligned with the direction of ground excitation. In contrast, elements are set to 0 when they do not align with the direction of ground excitation. Additionally, $S_{\ddot{x}_g}$ denotes the PSD of the ground motion acceleration.

To conduct the optimization, $S_{\ddot{x}_g}$ is substituted by a white noise S_0. Then, the PSD of the tower response under the white noise S_0, is given by:

$$\boldsymbol{S_{xx} = H(\omega) S_{pp} H(\omega)^{*T} = HMII^T M^T H^{*T} S_0} \tag{4-30}$$

The root mean square (RMS) value of displacement PSD, denoted as j, which is the area under the tower top displacement PSD curve, is defined as the objective function for the optimization.

$$j = \int_{-\infty}^{\infty} \boldsymbol{S_{xx}}\, d\omega \tag{4-31}$$

The PSD RMS (j) depends exclusively on two key variables: the natural frequency ratio (f) and the damping ratio of the oscillator (ξ_D). This dependency holds true as long as the main structure's parameters, mass ratio, negative stiffness ratio, and the intensity of the white noise input excitation are treated as predetermined and constant inputs. Consequently, the optimization problem be expressed mathematically as:

$$\begin{array}{c} \min j(f, \xi_D), \\ \hline \text{s.t. } R_k = 0, 0.5, 1, 1.5 \end{array} \tag{4-32}$$

The results of optimal parameters for the TMD are tabulated in Table 4-4, and the optimization results for the KDamper with different negative stiffness ratios ($R_k = 0.5, 1, 1.5$) are tabulated in

Table 4-5,

Table 4-6 and

Table 4-7, respectively.

Table 4-4. Parameters of optimized TMD

Frequency ratio f	Spring stiffness k_D (N/m)	Damping ratio ξ_D	Damping coefficient c_D (Ns/m)
0.951	56142	0.092	5149.1

Table 4-5. Parameters of optimized KDamper when $R_k = 0.5$

Connection configuration	Frequency ratio f	Positive spring stiffness $k_P\ (N/m)$	Negative spring stiffness $k_N\ (N/m)$	Damping ratio ξ_D	Damping coefficient $c_D\ (Ns/m)$
m_9	0.950	84036	-28012	0.099	5535.1
m_8	0.948	83682	-27894	0.107	5969.8
m_7	0.947	83506	-27835	0.113	6297.9
m_6	0.945	83153	-27718	0.119	6618.3
m_5	0.943	82802	-27601	0.125	6937.3
m_4	0.941	82451	-27484	0.129	7144.1
m_3	0.940	82276	-27425	0.132	7302.5
m_2	0.939	82101	-27367	0.135	7460.5
m_1	0.938	81926	-27309	0.136	7507.7
Ground	0.938	81926	-27309	0.137	7562.9

Table 4-6. Parameters of optimized KDamper when $R_k = 1.0$

Connection configuration	Frequency ratio f	Positive spring stiffness $k_P\ (N/m)$	Negative spring stiffness $k_N\ (N/m)$	Damping ratio ξ_D	Damping coefficient $c_D\ (Ns/m)$
m_9	0.949	111812	-55906	0.107	5976.1
m_8	0.946	111106	-55553	0.122	6792.3
m_7	0.943	110402	-55201	0.136	7547.8
m_6	0.940	109701	-54850	0.148	8187.6
m_5	0.937	109002	-54501	0.159	8768.1
m_4	0.933	108073	-54037	0.168	9224.8
m_3	0.930	107379	-53690	0.175	9578.3
m_2	0.928	106918	-53459	0.180	9830.8
m_1	0.927	106688	-53344	0.184	10038.4
Ground	0.926	106458	-53229	0.185	10082.1

Table 4-7. Parameters of optimized KDamper when $R_k = 1.5$

Connection configuration	Frequency ratio f	Positive spring stiffness $k_P\ (N/m)$	Negative spring stiffness $k_N\ (N/m)$	Damping ratio ξ_D	Damping coefficient $c_D\ (Ns/m)$
m_9	0.948	139470	-83682	0.115	6416.1
m_8	0.945	138589	-83153	0.137	7619.4
m_7	0.941	137418	-82451	0.159	8805.5
m_6	0.936	135962	-81577	0.178	9805.3
m_5	0.931	134513	-80708	0.196	10739.2
m_4	0.926	133072	-79843	0.210	11444.5
m_3	0.921	131639	-78983	0.221	11979.0

m_2	0.918	130783	-78470	0.230	12426.2
m_1	0.916	130213	-78128	0.235	12668.6
Ground	0.915	129929	-77958	0.236	12708.7

Charpter 5 Control effectiveness examination

5.1 Responses in the frequency domain

The responses of the MDoF system in the frequency domain are investigated in this section. In particular, the tower top PSD ($\boldsymbol{S_{xx}}$) under a given external excitation (S_0) as described in Equation (4-30) is taken out for analysis, and S_0 is set to be 1 for easy analysis. The control effectiveness of the ten different configurations of KDamper as discussed in Section 4.3 is evaluated against the traditional optimized TMD. Furthermore, a thorough comparisons between different KDamper configurations are also conducted.

Figure 5-1 displays the PSD of the displacement at the top of the wind turbine tower for three control scenarios: uncontrolled, with TMD installed, and with KDamper applied. For simplicity, only one KDamper configuration ($R_k = 1$, connected to m_5)) is shown. The peak value of the black curve, representing the resonant amplitude of the uncontrolled tower response, is observed at a frequency of 0.33 Hz, corresponding to the first natural frequency of the original tower.

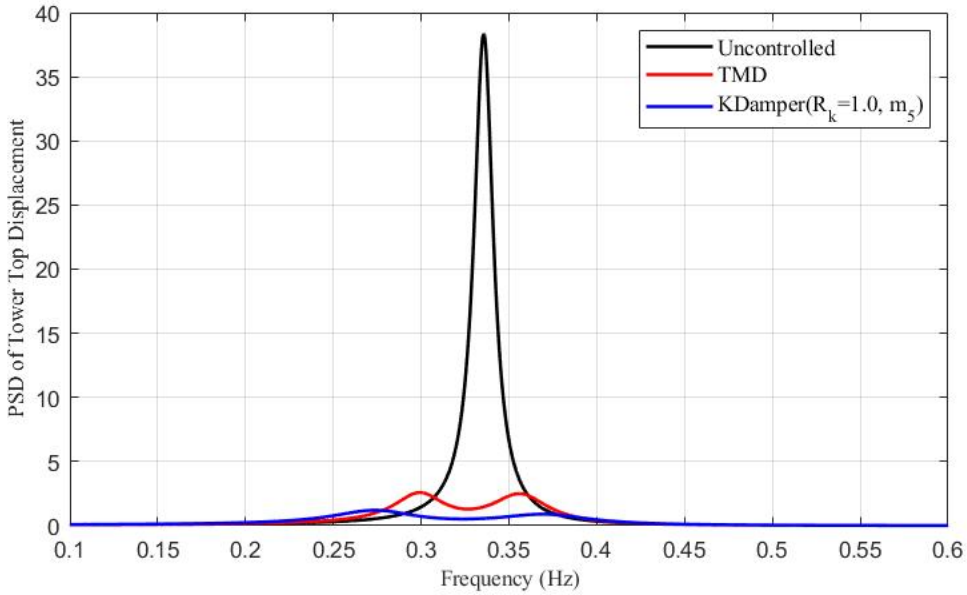

Figure 5-1. Displacement PSDs at the tower top.

It also can be seen from Figure 5-1 that after the installation of controlling devices (TMD or

KDamper), the tower responses have been drastically reduced, with a much less peak value and the under-curve area. To provide a clear demonstration of the effectiveness of TMD and KDamper, the values of the PSD RMS (j) of the tower response with different systems are tabulated in Table 5-1, Table 5-2, Table 5-3, and Table 5-4. The corresponding reduction ratios between the tower response with and without control devices are also provided in these tables. As shown in Table 5-1, the value of PSD RMS (j) for the uncontrolled system is 2113.9. When TMD is installed, the value of PSD RMS (j) reduce to 710.2, with the corresponding vibration reduction ratio of 66.40%.

Table 5-1. The PSD RMS (j) of the uncontrolled system and TMD

Uncontrolled system	TMD	
PSD RMS (j)	PSD RMS (j)	Reduction ratio (%)
2113.9	710.2	66.40

Table 5-2. The PSD RMS (j) of KDamper with reduction ratio when $R_k = 0.5$

Connection configuration	PSD RMS (j)	Reduction ratio compared to the original system (%)	Reduction ratio compared to TMD (%)
m_9	671.1	68.25	5.51
m_8	638.6	69.79	10.08
m_7	612.3	71.03	13.79
m_6	591.5	72.02	16.72
m_5	575.3	72.78	18.99
m_4	563.1	73.36	20.71
m_3	554.3	73.78	21.96
m_2	548.3	74.06	22.80
m_1	544.8	74.23	23.28
Ground	543.7	74.28	23.44

Table 5-3. The PSD RMS (j) of KDamper with reduction ratio when $R_k = 1.0$

Connection configuration	PSD RMS (j)	Reduction ratio compared to the original system (%)	Reduction ratio compared to TMD (%)
m_9	636.4	69.89	10.39
m_8	581.5	72.49	18.12
m_7	541.0	74.41	23.83
m_6	511.4	75.81	28.00

m_5	489.9	76.83	31.03
m_4	474.5	77.55	33.18
m_3	463.9	78.05	34.68
m_2	457.0	78.38	35.65
m_1	453.1	78.56	36.20
Ground	451.9	78.62	36.37

Table 5-4. The PSD RMS (j) of KDamper with reduction ratio when $R_k = 1.5$

Connection configuration	PSD RMS (j)	Reduction ratio compared to the original system (%)	Reduction ratio compared to TMD (%)
m_9	605.5	71.35	14.74
m_8	535.0	74.69	24.67
m_7	487.0	76.96	31.42
m_6	454.3	78.51	36.04
m_5	431.9	79.57	39.19
m_4	416.8	80.28	41.31
m_3	406.8	80.75	42.72
m_2	400.6	81.05	43.60
m_1	397.2	81.21	44.08
Ground	396.1	81.26	44.23

Also, according to Table 5-2, Table 5-3 and Table 5-4, the application of KDamper can provide even better vibration mitigation effectiveness than TMD, regardless of which configuration is adopted. The vibration mitigation effectiveness of KDamper depends on its configuration: the value of the negative stiffness ratio (R_k) and which mass point of the WT model that the negative stiffness element of KDamper is connected to. When the connected mass point is fixed, increasing the negative stiffness ratio (R_k) brings better vibration mitigation effectiveness. This conclusion can be drawn from the PSD curves shown in Figure 5-2(a), in which the PSD curve of KDamper with a higher R_k value presents a smaller under-curve area, which means a lower value of PSD RMS (j), which is confirmed by Figure 5-3. Meanwhile, with the same R_k value, downwards connection provides more effective vibration control. This conclusion can be drawn from the PSD curves shown in Figure 5-2(b), as well as from the decreasing trend of the value of PSD RMS (j), which are depicted in Figure 5-3. However, the improvement of control effectiveness is not proportional to the

increased downward connection intervals. As shown in Figure 5-2(b), with the same negative stiffness ratio $R_k = 1.0$, significantly reduced WT response is observed between the green PSD curve (connected to m_9) and the blue PSD curve (connected to m_5), but only minor improvement of the control effectiveness can be seen between the blue curve (connected to m_5) and the purple curve (connected to the ground). Moreover, according to Figure 4-2, the mass point m_5 locates at the mid-point of the WT model which means that the downward connection intervals from the tower top to m_5 are identical to the intervals from m_5 to ground, which is 43.8m. This conclusion can also be drawn from the reduction ratio compared to the uncontrolled system, as presented in Table 5-4. This table reveals that the value of PSD RMS (j), when connected to m_5 and to the ground, can provide a reduction ratio of 79.57% and 81.26% respectively, which means that only 1.69% improvement is achieved from the further downward connection from m_5 to the ground. Similar conclusions can be drawn from the reduction ratio when $R_k = 1.0$ and $R_k = 0.5$ as shown in Table 5-2 and Table 5-3. Apparently, the improvement of control effectiveness contributed by the further downward connection from m_5 to the ground cannot justify the subsequently increased material consumption and structural complexity. Thus, the configuration that $R_k = 1.5$ and connected to mass point m_5 is selected as the optimal configuration of KDamper, and will be applied to the simulation with actual seismic excitation in the time domain conducted in the next section.

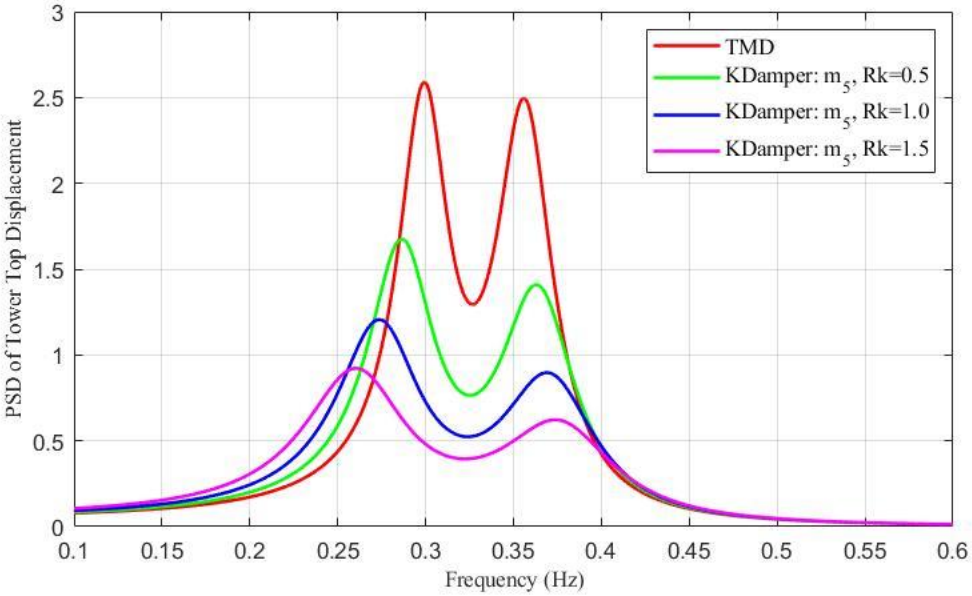

(a) Same connection position, different R_k value.

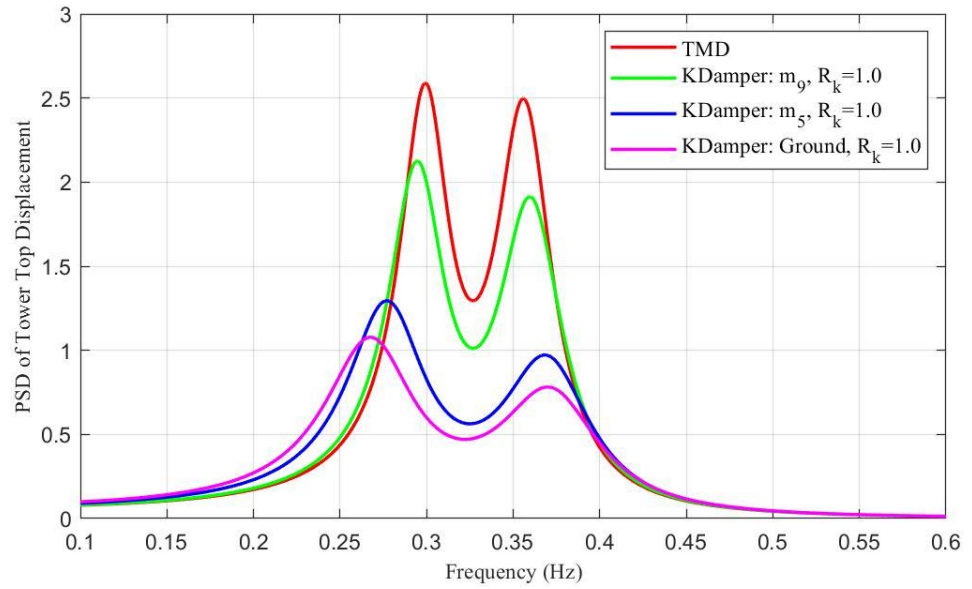

(b) Same R_k value, different connection position.

Figure 5-2. Displacement PSDs for TMD and KDamper with different configurations.

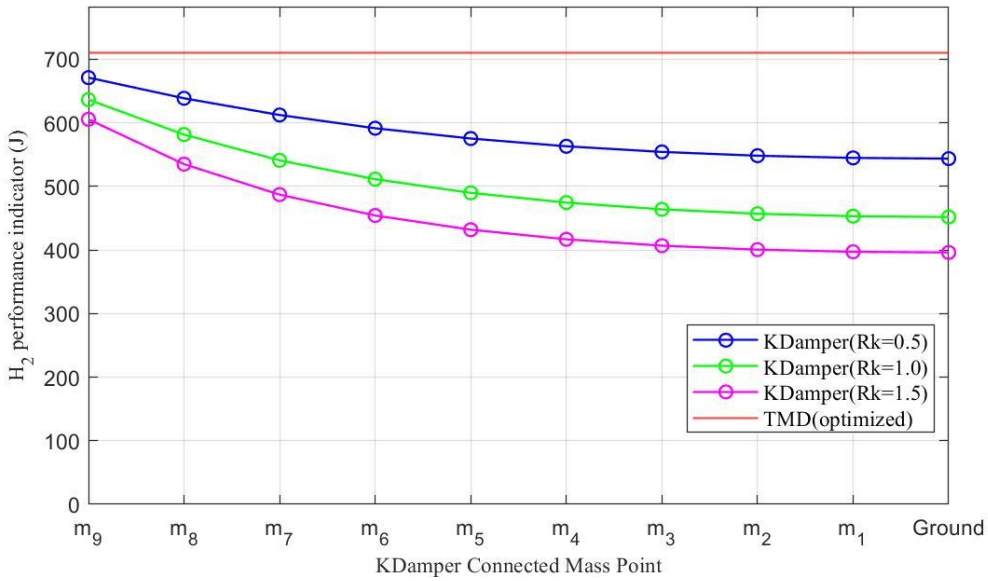

Figure 5-3. PSD RMS (j).

5.2 Responses in the time domain

5.2.1 Simulink model for solving the equation of motion

The mass, lateral stiffness and damping matrices for the uncontrolled and controlled are defined in Chapter 4. The motion equation (4-1) needs to be solved to get the dynamic response of the structure under certain external excitation ($\boldsymbol{x_g}$). A Simulink model is established in MATLAB based on Equation (4-1) to solve the differential motion equation as shown in Figure 5-4. The triangle block is the gain block to perform the matrix multiplication and the block with the symbol $\frac{1}{s}$ is the integrator block. The equations of motion for both the uncontrolled and controlled configurations are solved using the Runge-Kutta technique, specifically the 4th-order method (ode4 solver) as implemented in the Simulink software with a fixed time increment of 0.0001 seconds.

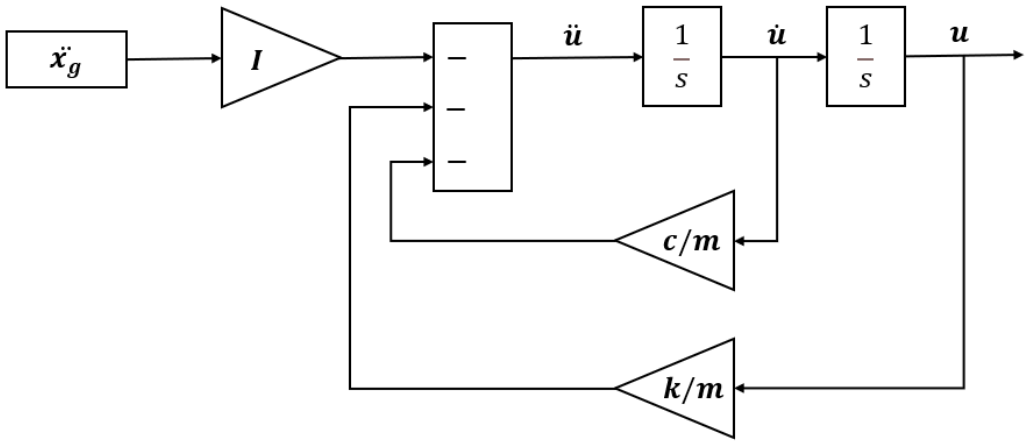

Figure 5-4. Simulink model for solving motion equations.

5.2.2 Selected seismic motions

To systematically examine the control performance of the proposed KDamper with the optimal configuration selected in Section 5.1 ($R_k = 1.5$, connected to mass point m_5), a set of 18 earthquake ground motion records has been chosen for the analysis. A detailed description of these selected seismic motions is presented in Table 5-5.

Table 5-5. Information of the selected earthquake ground motions.

No.	RSN	Earthquake Name	Station	Magnitude	R_{rup}(km)	V_{s30}(m/s)	PGA(g)
1	6	Imperial Valley-02	El Centro Array #9	6.95	6.09	213.44	0.281
2	15	Kern County	Taft Lincoln School	7.36	38.89	385.43	0.159
3	169	Imperial Valley-06	Delta	6.53	22.03	242.05	0.236
4	173	Imperial Valley-06	El Centro Array #10	6.53	8.60	202.85	0.173
5	180	Imperial Valley-06	El Centro Array #5	6.53	3.95	205.63	0.529
6	182	Imperial Valley-06	El Centro Array #7	6.53	0.56	210.51	0.341
7	728	Superstition Hills-02	Westmorland Fire Sta	6.54	13.03	193.67	0.173
8	779	Loma Prieta	LGPC	6.93	3.88	594.83	0.570
9	799	Loma Prieta	SF Intern. Airport	6.93	58.65	190.14	0.236
10	900	Landers	Yermo Fire Station	7.28	23.62	353.63	0.245
11	984	Northridge-01	LA - 116th St School	6.69	41.17	301.00	0.208
12	1044	Northridge-01	Newhall - Fire Sta	6.69	5.92	269.14	0.583
13	1107	Kobe, Japan	Kakogawa	6.90	22.50	312.00	0.240

14	1120	Kobe, Japan	Takatori	6.90	1.47	256.00	0.618
15	1540	Chi-Chi, Taiwan	TCU115	7.62	21.76	215.34	0.096
16	1633	Manjil, Iran	Abbar	7.37	12.55	723.95	0.515
17	5618	Iwate, Japan	IWT010	6.90	16.27	825.83	0.226
18	6890	Darfield, New Zealand	Christchurch Cashmere High School	7.00	17.64	204.00	0.229

Table 5-5 presents a chronological enumeration of the 18 ground motions employed to examine the performance of the KDamper system. These ground motions have been meticulously documented and acquired from the PEER ground motion database (https://ngawest2.berkeley.edu/). Due to the absence of specific seismic design codes for wind turbines, the selected seismic motions are scaled to conform with the average acceleration response spectrum outlined in the ASCE standard minimum design loads for buildings and other structures [74], utilizing a structural damping ratio of 5%. Figure 5-5 shows the good match between the scaled mean spectra and the target spectra, especially for the period equals to 3s, which is the period corresponding to the fundamental vibration mode of the WT model.

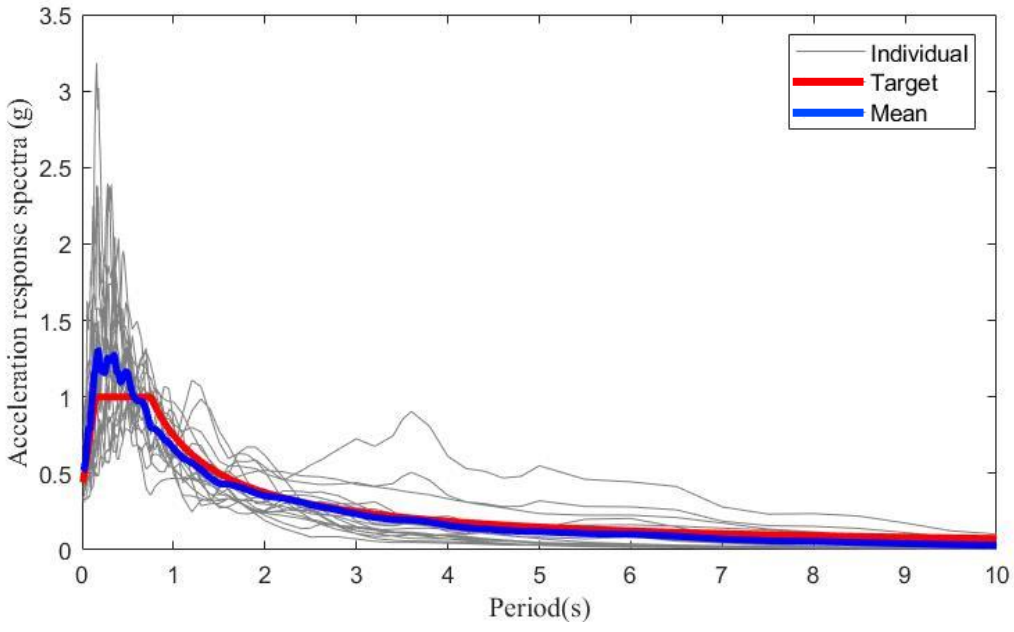

Figure 5-5. Acceleration response spectra.

5.2.3 Displacement response at the tower top

Figure 5-6 exhibits the displacement time histories at the top of the tower for both controlled and uncontrolled scenarios, subject to the influence of seismic motions No. 5. To maintain conciseness, the outcomes corresponding to the remaining earthquake ground motions are presented in the appendix (Figure A-1).

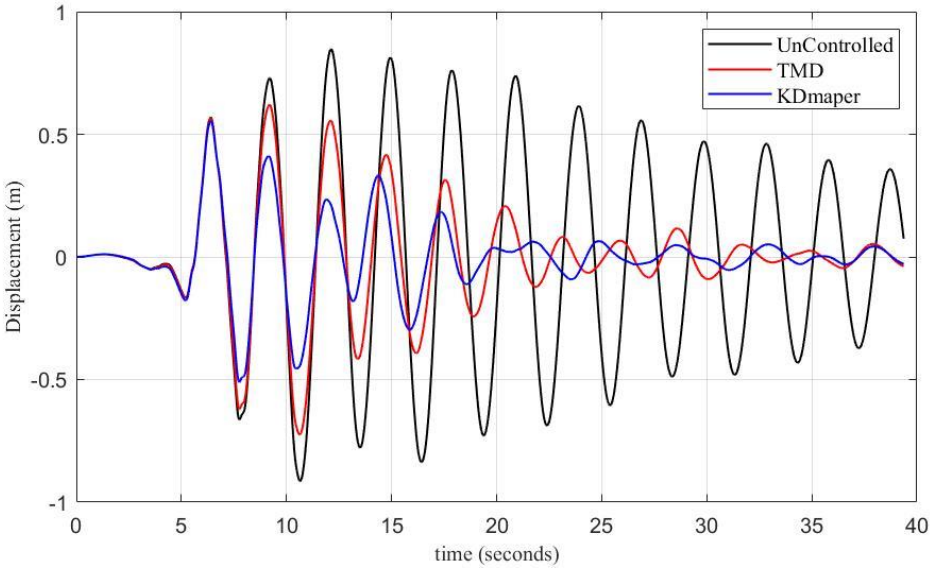

Figure 5-6. Displacement time history at the tower top with and without control for seismic input No. 5.

In general, the implementation of TMD and KDamper leads to a decrease in the displacement responses at the top of the tower, compared to the uncontrolled scenario. The degree of reduction varies with the specific seismic motion, highlighting the capacity of these control devices to enhance the structural integrity of wind turbine towers during seismic activity. Table 5-6 provides a comprehensive comparison of the maximum and RMS displacements at the top of the tower, serving as a means to evaluate the performance of the TMD and KDamper control measures. Furthermore, Figure 5-7 depicts the ratios of the maximum and RMS displacements between the tower response for both controlled and uncontrolled scenarios.

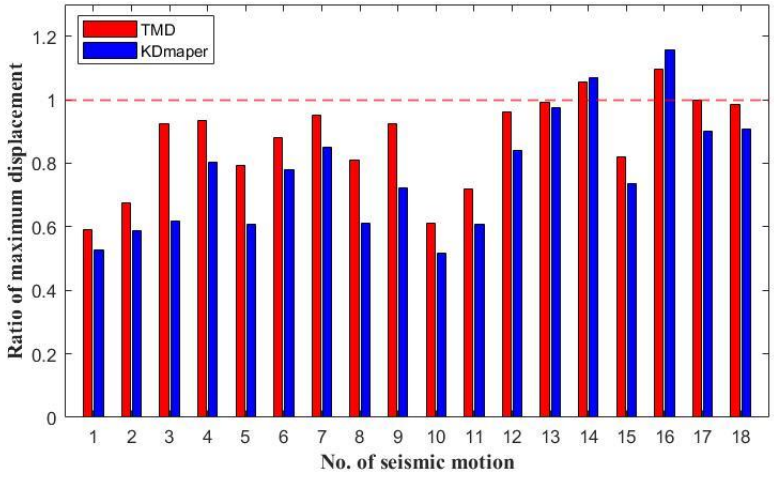

(a) Ratios of maximum displacements

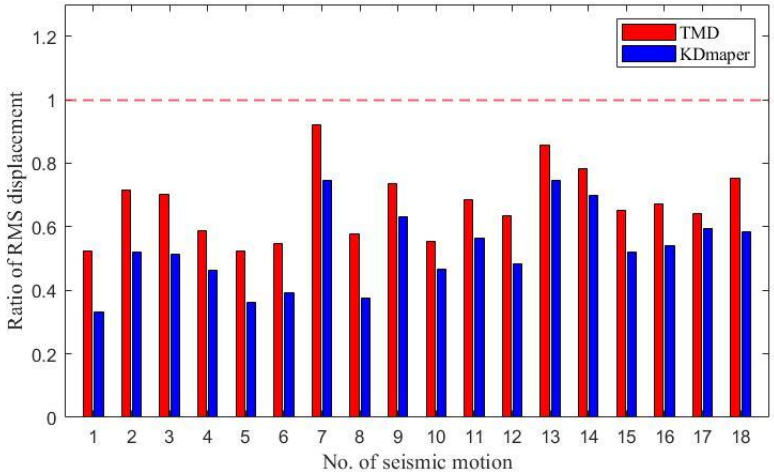

(b) Ratios of RMS displacements

Figure 5-7. Ratios of maximum and RMS displacement

The average ratios of the peak displacements with TMD and KDamper are 0.8736 and 0.7677, respectively, demonstrating that both TMD and KDamper can effectively suppress the peak displacement at the tower top, and KDamper can provide better vibration mitigation effectiveness in general except for seismic motion No. 14 and No. 16 as shown in Figure 5-7(a). This exception can be attributed to a variety of factors that challenge the performance of control devices. Primarily, these involve the potential for resonance and inappropriate tuning. Resonance can occur when the frequency of seismic motion aligns not with the natural frequency of the structure but with that of the control device, resulting in an increase in energy in the system and thus amplified displacement. Meanwhile, inappropriate tuning arises when the devices' parameters do not align optimally with the frequency of the seismic

event, potentially leading to an inadvertent addition of energy to the system, again causing an increase in displacement. Moreover, Table 5-6 and Figure 5-7(a) indicate that the effectiveness of TMD and KDamper in reducing the peak displacements is only marginal when the wind turbine model is exposed to seismic motions Nos. 7, 12, 13, 14, 16, 17, and 18. This observation can be attributed to the timing of the maximum displacements, which occur during the initial stages of the displacement time history for the aforementioned seismic motions, where the control devices do not exhibit significant effectiveness, as illustrated in Figure A-1 (f), (k), (l), (m), (o) and (p). However, in order to achieve effective control, the relative motion between the tower and control devices must develop, which requires a certain amount of time for the dampers to respond and generate relative deformation.

Table 5-6. Maximum and RMS displacement at the tower top with and without control

No.	Maximum displacement (m)			RMS displacement (m)		
	w/o control	TMD	KDamper	w/o control	TMD	KDamper
1	0.6391	0.3786	0.3374	0.2450	0.1281	0.0810
2	0.4603	0.3115	0.2709	0.1778	0.1270	0.0925
3	0.8306	0.7667	0.5132	0.2145	0.1510	0.1100
4	1.1876	1.1087	0.9537	0.5608	0.3295	0.2592
5	0.9143	0.7249	0.5555	0.4208	0.2200	0.1526
6	0.7919	0.6969	0.6181	0.3662	0.2004	0.1439
7	0.5763	0.5486	0.4901	0.2101	0.1937	0.1565
8	0.8408	0.6806	0.5135	0.4314	0.2494	0.1617
9	0.2024	0.1872	0.1460	0.0562	0.0413	0.0355
10	0.7494	0.4593	0.3882	0.2569	0.1420	0.1200
11	0.3868	0.2779	0.2350	0.1558	0.1066	0.0880
12	0.3902	0.3748	0.3282	0.1438	0.0911	0.0694
13	0.2819	0.2799	0.2747	0.0953	0.0816	0.0710
14	0.3244	0.3422	0.3473	0.1332	0.1041	0.0930
15	2.1739	1.7845	1.5984	0.6754	0.4402	0.3511
16	0.3895	0.4265	0.4503	0.1767	0.1188	0.0955
17	0.5255	0.5245	0.4727	0.0957	0.0615	0.0570
18	0.7173	0.7068	0.6514	0.1298	0.0975	0.0759

In comparison to the reduction of maximum displacements, TMD and KDamper are more effective in reducing the RMS displacements at the top of the tower. The average ratios of the RMS displacements for the wind turbine model equipped with TMD and KDamper are 0.6345 and 0.4871, respectively. Notably, KDamper exhibits better performance than TMD

across all tested seismic motions.

5.2.4 Acceleration response on the tower top

Most of the mechanical and electrical components of wind turbines, such as rotary mechanisms and generators, are sensitive to accelerations. Thus, it is necessary to investigate the control effectiveness of TMD and KDamper on acceleration responses as well.

Figure 5-8 displays the acceleration time histories at the top of the tower when the wind turbine model is subjected to seismic motions No. 5. The RMS acceleration response under all examined ground motions is tabulated in Table 5.7. Moreover, the ratios between the controlled and uncontrolled configurations for these RMS accelerations are illustrated in Figure 5-9. The RMS acceleration response for all tested ground motions is reduced by control devices KDamper and TMD.

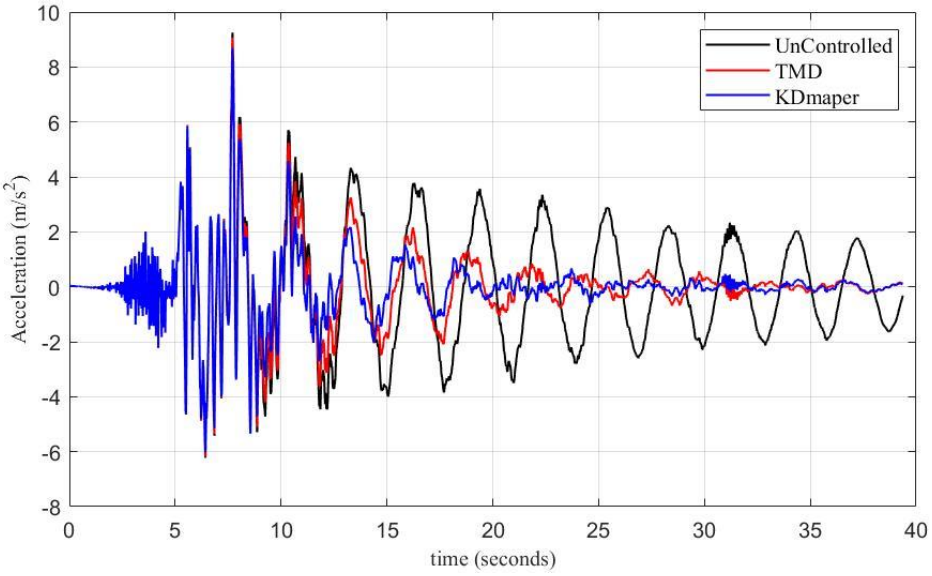

Figure 5-8. Acceleration time history at the tower top with and without control for seismic input No. 5.

Table 5-7. RMS accelerations at the tower top (unit in m/s^2)

No.	w/o control	TMD	KDamper
1	1.4114	1.0736	0.9671
2	1.3669	1.2439	1.1743
3	1.3553	1.1748	1.0856

4	2.6385	1.6163	1.2698
5	2.1344	1.4124	1.1804
6	1.7915	1.1470	0.9528
7	1.3395	1.2738	1.1042
8	2.1939	1.5196	1.2347
9	1.0094	0.9961	0.9936
10	1.3852	1.0139	0.9468
11	1.4427	1.3561	1.3301
12	1.2027	1.1015	1.0755
13	1.3160	1.2948	1.2907
14	1.0331	0.9675	0.9663
15	3.0029	1.8658	1.4255
16	1.5265	1.4204	1.3826
17	0.7056	0.6322	0.6289
18	0.7542	0.6535	0.5865

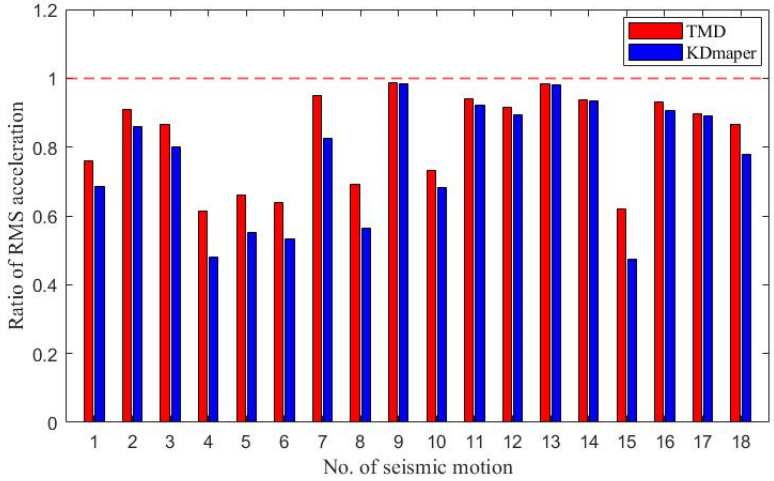

Figure 5-9. Ratios of RMS accelerations at the tower top

Overall, the KDamper demonstrates superior performance compared to the TMD across all examined ground motions. The reduction ratios for the KDamper are contingent upon the specific seismic motions being assessed, indicating a varying degree of effectiveness depending on the earthquake input, which can be explained by analyzing the Fast Fourier Transform (FFT) of the acceleration response time series of the uncontrolled tower, as depicted in Figure 5-10.

In the present study, the effectiveness of the KDamper in mitigating the acceleration response of a wind turbine tower under different seismic excitations was evaluated by the reduction

ratios. For conciseness, four gound motions are analysed by FFT in detail, i.e., No.4, No.9, No.13 and No.15, with earthquake No.4 and No.15 exhibiting the best control effectiveness, and earthquake No.9 and No.13 showing the worst performance. The FFT plots of the acceleration response of the uncontrolled tower under these excitations, as presented in Figure 5-10, provided further insights into the control effectiveness. Figure 5-10 (a) and (b) revealed that the frequency content near the 1st modal frequency of the uncontrolled tower (0.33Hz) had a relatively high amplitude under earthquake No.4 and No.15, indicating effective control. This is consistent with the fact that the mechanical characteristics of both the TMD and KDamper are optimized with respect to the fundamental frequency of the tower. However, as shown in Figure 5-10 (c) and (d), under earthquake No.9 and No.13, the scattered frequency content of the acceleration response in the 1st-2nd modal frequency range (0.33-3Hz) made it difficult for the KDamper to suppress the vibration effectively. This result is consistent with the reduction ratios presented in Figure 5-9, which were less than 0.05 for these two excitations.

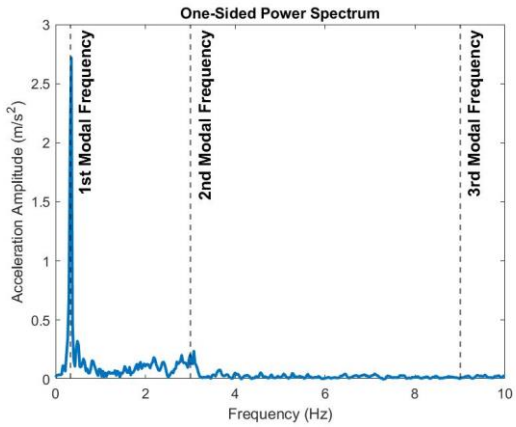

(a) No. 4

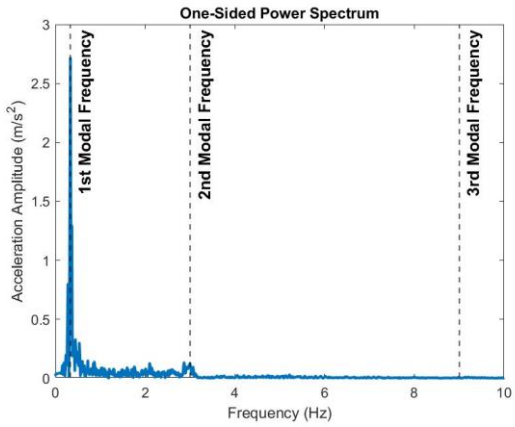

(b) No. 15

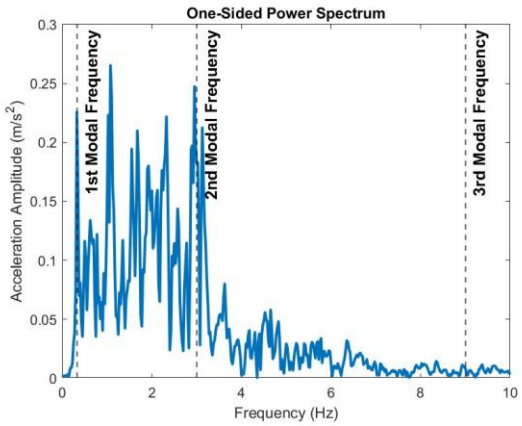

(c) No. 9

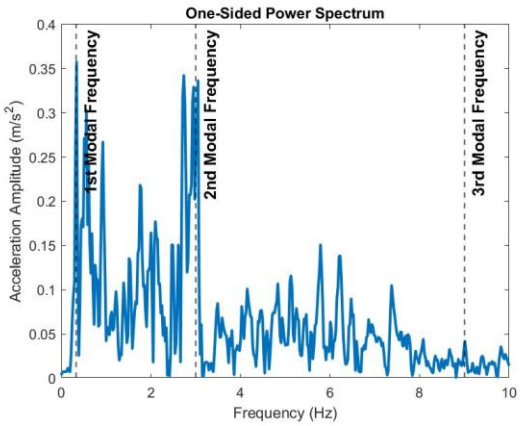

(d) No. 13

Figure 5-10. FFT of the acceleration response of the uncontrolled tower under the Nos. 9, 13, and 16 inputs.

Moreover, the location of the control devices is critical to their effectiveness. In this study, the control devices were placed at the top of the tower, which aligns with the height of the peak amplitude of the 1st modal shape. However, as illustrated in Figure 4-3, the maximum amplitude of the second mode shape occurs approximately 40 meters below the top of the tower. Thus, when the tower is subjected to seismic excitations with frequency contents other than the fundamental frequency of the uncontrolled tower, the relatively minor acceleration response at the top of the tower restricts the ability of KDamper and TMD to control the response. This is because the control efficiency of these devices is typically dependent on the amplitude of the excitation.

In general, the KDamper has demonstrated better performance than the TMD in controlling the RMS accelerations of the wind turbine tower. The average ratios of the RMS accelerations with KDamper and TMD are 0.7097 and 0.7882, respectively. This suggests that KDamper's control ability in reducing the acceleration responses for different ground motion inputs is consistent with its performance in reducing the RMS displacements. The results indicate that the KDamper is a more effective control device than the TMD for reducing the RMS accelerations and displacements of the wind turbine tower under seismic excitations.

5.2.5 Robustness

As mentioned before, the natural frequencies of a wind turbine can be affected by various factors during its service life, including environmental factors, such as soil-structure interaction (SSI), scouring and liquefication, and operational factors, such as components aging and fatigue. Previous research [75-77] has reported notable differences in the first fore-aft frequencies of wind turbine towers with and without Soil-Structure Interaction (SSI), including a 15% difference in Ref. [75], a 31% difference in Ref. [76], and a 47% difference in Ref. [77]. It is evident that these variations are reliant on the geometric parameters of the monopile foundation and the properties of the underlying soil.

Moreover, the natural frequencies of wind turbine towers would be further changed by scouring [78] caused by cyclic wind, and soil liquefication [79] induced by seismic loads. In addition, the aging, rusting and fatigue of certain components, such as connectors and fasteners, can further contribute to the deviation of natural frequencies of wind turbine towers.

To test and verify the performance and stability of proposed control devices under shifted structural frequencies, the fundamental frequency of the wind turbine tower model is altered within the range of -30% to +30%, with an interval of 5%. The frequency shifting is achieved by adjusting the structural stiffness.

All 18 ground motions are tested under shifted structural frequencies, their ratio of RMS displacements and accelerations are recorded in Figure A-3 and Figure A-4. Table 5-8 tabulates the averaged RMS displacements and accelerations for all 18 tested ground motions with investigated structural frequencies, and the ratios of the RMS displacement and acceleration between controlled and uncontrolled tower configurations under each shifted structural frequency are averaged and presented in Figure 5-11. For comparison, the averaged ratio of the RMS displacement and acceleration under the original frequency is also presented in this figure.

As shown in Figure 5-11, the KDamper and TMD can still suppress the RMS displacements and accelerations response at the tower top under all shifted structural frequencies, and the

KDamper outperforms the TMD counterpart for both RMS displacement and acceleration ratios under all investigated frequency ratios.

According to Figure 5-11 (a) and Table 5-8, under the original structural frequency, the average RMS displacements are 0.1602 m and 0.1230 m for TMD and KDamper respectively, and the corresponding response ratios are 0.6345 and 0.4871. While under the most unfavourable shifted structural frequency ratio, i.e., -30%, the average RMS displacements are 0.2751 m and 0.2076 m for TMD and KDamper respectively, and the corresponding response ratios are 0.8926 and 0.6738. KDamper provides substantial reductions in the RMS displacements under all shifted structural frequencies, and the increase of the response ratio between the most unfavourable structural frequency and the original frequency is 0.1867. However, TMD becomes almost ineffective when the structural frequency is shifted by -30%, and the increase of the response ratio between the most unfavourable structural frequency and the original frequency is 0.2581. Thus, KDamper presents better robustness than TMD for RMS displacement responses.

Similarly, as shown in Figure 5-11 (b) and Table 5-8, under the original structural frequency, the average RMS accelerations are 1.1291 m/s^2 and 1.0886 m/s^2 for TMD and KDamper, respectively, and the corresponding response ratios are 0.7882 and 0.7097. While under the most unfavourable shifted structural frequency ratio, i.e., -30%, the average RMS accelerations are 1.1162 m/s^2 and 0.9942 m/s^2 for TMD and KDamper respectively, and the corresponding response ratios are 0.9402 and 0.8375. The increase of the RMS acceleration response ratio between the most unfavourable structural frequency and the original frequency are 0.1520 and 0.1278 for TMD and KDamper respectively, indicating that KDamper also outperforms TMD in the robustness of RMS acceleration response.

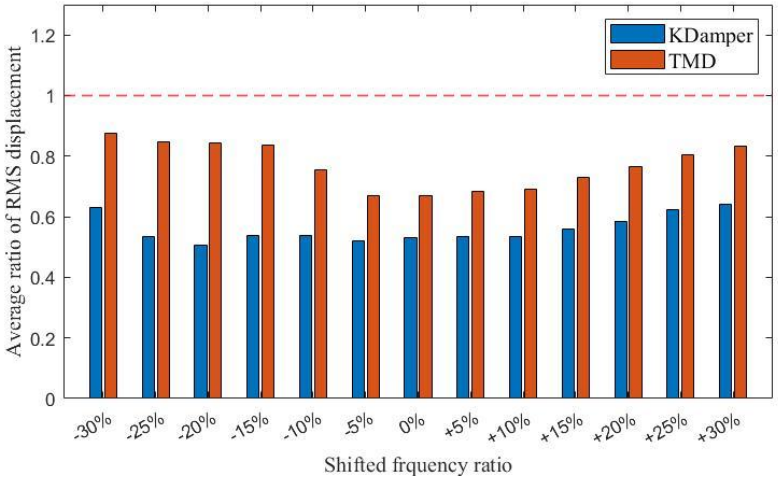

(a) Averaged displacement ratios

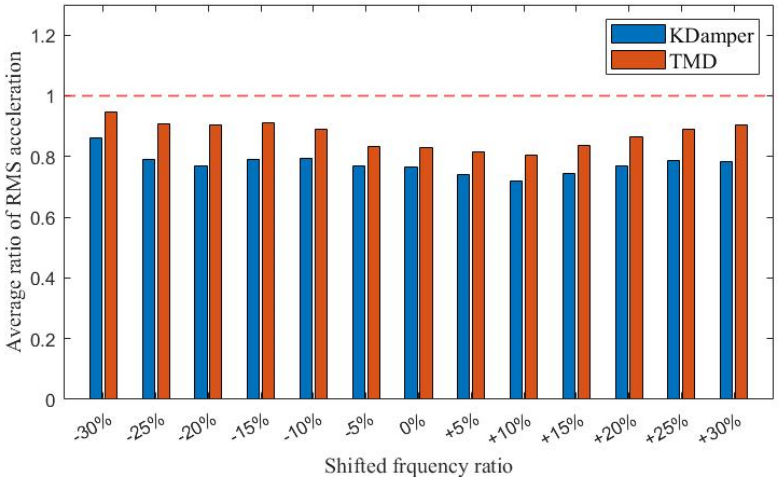

(b) Averaged acceleration ratios

Figure 5-11. Averaged ratios of RMS displacements and accelerations under different structural frequencies

Table 5-8. Averaged RMS displacements and accelerations under different structural frequencies

Shifted structural frequency ratio	Displacement (m)			Acceleration (m/s2)		
	Uncontrolled	TMD	KDamper	Uncontrolled	TMD	KDamper
-30%	0.3082	0.2751	0.2076	1.1871	1.1162	0.9942
-25%	0.3461	0.2822	0.1776	1.3263	1.1703	0.9818
-20%	0.3586	0.2859	0.1591	1.4642	1.2548	1.0009
-15%	0.3082	0.2563	0.1485	1.4261	1.2652	1.0244
-10%	0.2577	0.2073	0.1392	1.3564	1.2143	1.0500
-5%	0.2555	0.1728	0.1302	1.4478	1.1866	1.0733
0%	0.2525	0.1602	0.1230	1.5339	1.2091	1.0886
5%	0.2543	0.1596	0.1182	1.6447	1.2732	1.1199
10%	0.2529	0.1579	0.1151	1.7120	1.2983	1.1303

15%	0.2213	0.1535	0.1131	1.6393	1.3380	1.1706
20%	0.2008	0.1504	0.1125	1.6161	1.3801	1.2132
25%	0.1871	0.1489	0.1136	1.6118	1.4246	1.2515
30%	0.1847	0.1532	0.1150	1.6975	1.5263	1.3072

Charpter 6 Conclusions and future works

6.1 Main findings

This thesis studies the dynamic performance of using KDamper to control the tower vibrations of wind turbines when they are subjected to earthquake excitations, with modified installation configurations. The influences of mechanical parameters of the KDamper, including mass ratio, damping coefficient and negative stiffness ratio are numerically and analytically investigated. Moreover, the vibration mitigation effectiveness of the KDamper is compared with that of a traditional TMD with similar parameters. Furthermore, the dynamic performance of KDamper and TMD under various seismic excitations are numerically studied and compared, and the robustness of controlling devices with different structural frequencies is discussed.

Chapter 3 investigates the influences of different mechanical parameters, including mass ratio, damping ratio and negative stiffness ratio, on KDamper's dynamic performance. Analytical study of KDamper reveals its three basic properties:

1. With an equal mass ratio, KDamper always provides a better effect of vibration mitigation compared to TMD.
2. Instead of increasing auxiliary mass, KDamper can achieve a better vibration isolation effect by increasing the absolute value of the negative stiffness element.
3. The augmentation of the Negative Stiffness Element is subject to an upper limit determined by the static stability of the structure.

In Chapter 4, the NREL 5MW wind turbine is adapted as the investigated model for this research. Lumped mass simplification and control device application are performed, and optimal parameters are obtained for different configurations.

Chapter 5 numerically investigates the vibration mitigation performance of KDamper and TMD in both the frequency domain and time domain. In the frequency domain, it is found

that a downward connection of the negative stiffness element leads to better vibration mitigation effectiveness. However, the improvement of control effectiveness is not proportional to the increased downward connection intervals. Thus, connecting to the mid-point of the tower is selected as the configuration to perform simulation under the time domain. Then, 18 earthquakes are adapted as the external excitation for the simulation under the time domain. Numerical results reveal that:

1. Both TMD and KDamper are more effective in reducing the RMS displacements at the tower top compared with the reduction of maximum displacements. KDamper outperforms TMD in all tested ground motions.
2. KDamper exhibits better performance than TMD for all tested ground motions in terms of suppressing RMS accelerations. However, when the tower is subjected to seismic motions that are governed by the second or third mode, the control performance of KDamper is limited.
3. KDamper presents better robustness than TMD for both RMS displacement and RMS acceleration responses under all investigated structural frequencies.

6.2 Recommendations for future works

In this thesis, the performance of applying KDamper to a wind turbine model for vibration mitigation is quantified and discussed. However, the negative stiffness element of the KDamper is assumed to be a constant value in this research. In fact, negative stiffness dampers are normally realized by springs, beams and magnetism devices with non-linear characteristics [36]. Thus, it is necessary to develop a prototype of the negative stiffness vibration isolation device and carry out analytical studies to simulate the dynamic behaviour device. Moreover, if the performance of the prototype device can be verified by simulation, producing the device using 3D printing and carrying out the shake table test is also deemed necessary for future investigations.

References

1. Bath, A., *Global Wind Report 2023*. 2023, Global Wind Energy Council: Brussels, Belgium.
2. Jonkman, J., et al., *Definition of a 5-MW reference wind turbine for offshore system development*. 2009, National Renewable Energy Lab.(NREL), Golden, CO (United States).
3. Chou, J.-S. and W.-T. Tu, *Failure analysis and risk management of a collapsed large wind turbine tower.* Engineering Failure Analysis, 2011. **18**(1): p. 295-313.
4. Zuo, H., K. Bi, and H. Hao, *A state-of-the-art review on the vibration mitigation of wind turbines.* Renewable and Sustainable Energy Reviews, 2020. **121**: p. 109710.
5. Rahman, M., et al., *Performance enhancement of wind turbine systems with vibration control: A review.* Renewable & Sustainable Energy Reviews, 2015. **51**: p. 43-54.
6. Staino, A. and B. Basu, *Dynamics and control of vibrations in wind turbines with variable rotor speed.* Engineering Structures, 2013. **56**: p. 58-67.
7. Krenk, S., M.N. Svendsen, and J. Høgsberg, *Resonant vibration control of three-bladed wind turbine rotors.* AIAA journal, 2012. **50**(1): p. 148-161.
8. Maldonado, V., et al., *Active Vibration Control of a Wind Turbine Blade Using Synthetic Jets.* International Journal of Flow Control, 2009. **1**(4).
9. Rezaee, M. and A.M. Aly, *Vibration control in wind turbines to achieve desired system-level performance under single and multiple hazard loadings.* Structural Control and Health Monitoring, 2018. **25**(12): p. e2261.
10. Martynowicz, P., *Vibration control of wind turbine tower-nacelle model with magnetorheological tuned vibration absorber.* Journal of Vibration and Control, 2017. **23**(20): p. 3468-3489.
11. Park, S., et al., *An investigation on the impacts of passive and semiactive structural control on a fixed bottom and a floating offshore wind turbine.* Wind Energy, 2019. **22**(11): p. 1451-1471.
12. Murtagh, P., et al., *Passive control of wind turbine vibrations including blade/tower interaction and rotationally sampled turbulence.* Wind Energy: An International Journal for Progress and Applications in Wind Power Conversion Technology, 2008. **11**(4): p. 305-317.
13. Lackner, M.A. and M.A. Rotea, *Passive structural control of offshore wind turbines.* Wind energy, 2011. **14**(3): p. 373-388.
14. Stewart, G. and M. Lackner, *Offshore wind turbine load reduction employing optimal passive tuned mass damping systems.* IEEE transactions on control systems technology, 2013. **21**(4): p. 1090-1104.

15. Stewart, G.M. and M.A. Lackner, *The impact of passive tuned mass dampers and wind–wave misalignment on offshore wind turbine loads.* Engineering structures, 2014. **73**: p. 54-61.

16. Tong, X., X. Zhao, and S. Zhao, *Load reduction of a monopile wind turbine tower using optimal tuned mass dampers.* International Journal of Control, 2017. **90**(7): p. 1283-1298.

17. Zuo, H., K. Bi, and H. Hao, *Using multiple tuned mass dampers to control offshore wind turbine vibrations under multiple hazards.* Engineering Structures, 2017. **141**: p. 303-315.

18. Hemmati, A., E. Oterkus, and M. Khorasanchi, *Vibration suppression of offshore wind turbine foundations using tuned liquid column dampers and tuned mass dampers.* Ocean Engineering, 2019. **172**: p. 286-295.

19. Tong, X., X. Zhao, and A. Karcanias, *Passive vibration control of an offshore floating hydrostatic wind turbine model.* Wind Energy, 2018. **21**(9): p. 697-714.

20. Hochrainer, M.J. and F. Ziegler, *Control of tall building vibrations by sealed tuned liquid column dampers.* Structural Control and Health Monitoring: The Official Journal of the International Association for Structural Control and Monitoring and of the European Association for the Control of Structures, 2006. **13**(6): p. 980-1002.

21. Dezvareh, R., K. Bargi, and S.A. Mousavi, *Control of wind/wave-induced vibrations of jacket-type offshore wind turbines through tuned liquid column gas dampers.* Structure and Infrastructure Engineering, 2016. **12**(3): p. 312-326.

22. Bargi, K., R. Dezvareh, and S.A. Mousavi, *Contribution of tuned liquid column gas dampers to the performance of offshore wind turbines under wind, wave, and seismic excitations.* Earthquake Engineering and Engineering Vibration, 2016. **15**(3): p. 551-561.

23. Chen, J.-L. and C.T. Georgakis, *Spherical tuned liquid damper for vibration control in wind turbines.* Journal of Vibration and Control, 2015. **21**(10): p. 1875-1885.

24. Ghaemmaghami, A., R. Kianoush, and X.X. Yuan, *Numerical modeling of dynamic behavior of annular tuned liquid dampers for applications in wind towers.* Computer-Aided Civil and Infrastructure Engineering, 2013. **28**(1): p. 38-51.

25. Ha, M. and C. Cheong, *Pitch motion mitigation of spar-type floating substructure for offshore wind turbine using multilayer tuned liquid damper.* Ocean Engineering, 2016. **116**: p. 157-164.

26. Zhang, Z., et al., *Performance evaluation of full-scale tuned liquid dampers (TLDs) for vibration control of large wind turbines using real-time hybrid testing.* Engineering Structures, 2016. **126**: p. 417-431.

27. Zhang, Z., B. Basu, and S.R. Nielsen, *Real-time hybrid aeroelastic simulation of wind turbines with various types of full-scale tuned liquid dampers.* Wind Energy, 2019. **22**(2):

p. 239-256.

28. Colwell, S. and B. Basu, *Tuned liquid column dampers in offshore wind turbines for structural control.* Engineering Structures, 2009. **31**(2): p. 358-368.
29. Mensah, A.F. and L. Dueñas-Osorio, *Improved reliability of wind turbine towers with tuned liquid column dampers (TLCDs).* Structural Safety, 2014. **47**: p. 78-86.
30. Chen, J., Y. Liu, and X. Bai, *Shaking table test and numerical analysis of offshore wind turbine tower systems controlled by TLCD.* Earthquake Engineering and Engineering Vibration, 2015. **14**(1): p. 55-75.
31. Chen, J. and C.T. Georgakis, *Tuned rolling-ball dampers for vibration control in wind turbines.* Journal of Sound and Vibration, 2013. **332**(21): p. 5271-5282.
32. Zhang, Z.-L., J.-B. Chen, and J. Li, *Theoretical study and experimental verification of vibration control of offshore wind turbines by a ball vibration absorber.* Structure and Infrastructure Engineering, 2014. **10**(8): p. 1087-1100.
33. Molyneux, W., *Supports for vibration isolation.* 1957.
34. Platus, D.L. *Negative-stiffness-mechanism vibration isolation systems*. in *Vibration control in microelectronics, optics, and metrology*. 1992. SPIE.
35. Carrella, A., M. Brennan, and T. Waters, *Static analysis of a passive vibration isolator with quasi-zero-stiffness characteristic.* Journal of sound and vibration, 2007. **301**(3-5): p. 678-689.
36. Li, H., Y. Li, and J. Li, *Negative stiffness devices for vibration isolation applications: a review.* Advances in Structural Engineering, 2020. **23**(8): p. 1739-1755.
37. Le, T.D. and K.K. Ahn, *A vibration isolation system in low frequency excitation region using negative stiffness structure for vehicle seat.* Journal of Sound and Vibration, 2011. **330**(26): p. 6311-6335.
38. Le, T.D. and K.K. Ahn, *Experimental investigation of a vibration isolation system using negative stiffness structure.* International Journal of Mechanical Sciences, 2013. **70**: p. 99-112.
39. Le, T.D. and K.K. Ahn, *Fuzzy sliding mode controller of a pneumatic active isolating system using negative stiffness structure.* Journal of Mechanical Science and Technology, 2012. **26**(12): p. 3873-3884.
40. Niu, F., et al., *Design and analysis of a quasi-zero stiffness isolator using a slotted conical disk spring as negative stiffness structure.* Journal of Vibroengineering, 2014. **16**(4): p. 1769-1785.
41. Liu, X., X. Huang, and H. Hua, *On the characteristics of a quasi-zero stiffness isolator using Euler buckled beam as negative stiffness corrector.* Journal of Sound and Vibration, 2013. **332**(14): p. 3359-3376.

42. Huang, X., et al., *Vibration isolation characteristics of a nonlinear isolator using Euler buckled beam as negative stiffness corrector: a theoretical and experimental study.* Journal of Sound and Vibration, 2014. **333**(4): p. 1132-1148.

43. Xu, D., et al., *Theoretical and experimental analyses of a nonlinear magnetic vibration isolator with quasi-zero-stiffness characteristic.* Journal of sound and vibration, 2013. **332**(14): p. 3377-3389.

44. Nagarajaiah, S., et al. *Adaptive negative stiffness: a new structural modification approach for seismic protection*. in *Advanced Materials Research*. 2013. Trans Tech Publ.

45. Pasala, D., et al., *Adaptive negative stiffness: new structural modification approach for seismic protection.* Journal of structural Engineering, 2013. **139**(7): p. 1112-1123.

46. Sarlis, A., et al., *Negative stiffness device for seismic protection of structures: shake table testing of a seismically isolated structure.* Journal of Structural Engineering, 2016(5): p. 04016005.

47. Attary, N., et al. *Performance assessment of a highway bridge structure employing adaptive negative stiffness for seismic protection*. in *Structures Congress*. 2013.

48. Attary, N., et al., *Performance evaluation of negative stiffness devices for seismic response control of bridge structures via experimental shake table tests.* Journal of Earthquake Engineering, 2015. **19**(2): p. 249-276.

49. Attary, N., et al., *Numerical simulations of a highway bridge structure employing passive negative stiffness device for seismic protection.* Earthquake Engineering & Structural Dynamics, 2015. **44**(6): p. 973-995.

50. IEMURA, H., et al. *Development of the passive negative stiffness friction device and its verification tests through shaking table*. in *Proceedings of the JSCE Earthquake Engineering Symposium*. 2007. Japan Society of Civil Engineers.

51. Antoniadis, I., et al., *Hyper-damping properties of a stiff and stable linear oscillator with a negative stiffness element.* Journal of Sound and Vibration, 2015. **346**: p. 37-52.

52. Antoniadis, I.A., et al., *KDamping: A stiffness based vibration absorption concept.* Journal of Vibration and Control, 2018. **24**(3): p. 588-606.

53. Sapountzakis, I.E., P.G. Tranakidis, and I.A. Antoniadis, *Implementation of the KDamper concept using disc springs.* Journal of Low Frequency Noise, Vibration and Active Control, 2019. **38**(1): p. 168-186.

54. Sapountzakis, E., et al., *KDamper concept in seismic isolation of bridges with flexible piers.* Engineering Structures, 2017. **153**: p. 525-539.

55. Kapasakalis, K., E. Sapountzakis, and I. Antoniadis. *Implementation of the KDamper concept to wind turbine towers*. in *Proceedings of the 6th international conference on computational methods in structural dynamics and earthquake engineering (COMPDYN*

2017). 2017.

56. Murtagh, P., B. Basu, and B. Broderick, *Along-wind response of a wind turbine tower with blade coupling subjected to rotationally sampled wind loading.* Engineering structures, 2005. **27**(8): p. 1209-1219.
57. Chopra, A.K., *Dynamics of structures*. 1975, Pearson Prentice Hall Hoboken.
58. Arany, L., et al., *Closed form solution of Eigen frequency of monopile supported offshore wind turbines in deeper waters incorporating stiffness of substructure and SSI.* Soil Dynamics and Earthquake Engineering, 2016. **83**: p. 18-32.
59. Koukoura, C., A. Natarajan, and A. Vesth, *Identification of support structure damping of a full scale offshore wind turbine in normal operation.* Renewable Energy, 2015. **81**: p. 882-895.
60. Katsanos, E.I., S. Thöns, and C.T. Georgakis, *Wind turbines and seismic hazard: a state-of-the-art review.* Wind Energy, 2016. **19**(11): p. 2113-2133.
61. Den Hartog, J.P., *Mechanical vibrations*. 1985: Courier Corporation.
62. Abé, M. and Y. Fujino, *Dynamic characterization of multiple tuned mass dampers and some design formulas.* Earthquake engineering & structural dynamics, 1994. **23**(8): p. 813-835.
63. Warburton, G.B., *Optimum absorber parameters for various combinations of response and excitation parameters.* Earthquake Engineering & Structural Dynamics, 1982. **10**(3): p. 381-401.
64. Yamaguchi, H. and N. Harnpornchai, *Fundamental characteristics of multiple tuned mass dampers for suppressing harmonically forced oscillations.* Earthquake engineering & structural dynamics, 1993. **22**(1): p. 51-62.
65. Sadek, F., et al., *A method of estimating the parameters of tuned mass dampers for seismic applications.* Earthquake Engineering & Structural Dynamics, 1997. **26**(6): p. 617-635.
66. Jangid, R., *Optimum multiple tuned mass dampers for base-excited undamped system.* Earthquake engineering & structural dynamics, 1999. **28**(9): p. 1041-1049.
67. Li, C., *Optimum multiple tuned mass dampers for structures under the ground acceleration based on DDMF and ADMF.* Earthquake engineering & structural dynamics, 2002. **31**(4): p. 897-919.
68. Bakre, S. and R. Jangid, *Optimum multiple tuned mass dampers for base-excited damped main system.* International Journal of Structural Stability and Dynamics, 2004. **4**(04): p. 527-542.
69. Bakre, S. and R. Jangid, *Optimum parameters of tuned mass damper for damped main system.* Structural Control and Health Monitoring: The Official Journal of the International Association for Structural Control and Monitoring and of the European

Association for the Control of Structures, 2007. **14**(3): p. 448-470.

70. Hoang, N., Y. Fujino, and P. Warnitchai, *Optimal tuned mass damper for seismic applications and practical design formulas.* Engineering structures, 2008. **30**(3): p. 707-715.
71. Bi, K. and H. Hao, *Using pipe-in-pipe systems for subsea pipeline vibration control.* Engineering Structures, 2016. **109**: p. 75-84.
72. Kampitsis, A., K. Kapasakalis, and L. Via-Estrem, *An integrated FEA-CFD simulation of offshore wind turbines with vibration control systems.* Engineering Structures, 2022. **254**: p. 113859.
73. Datta, T.K., *Seismic analysis of structures*. 2010: John Wiley & Sons.
74. Engineers, A.S.o.C. *Minimum design loads and associated criteria for buildings and other structures*. 2017. American Society of Civil Engineers.
75. Abdullahi, A., Y. Wang, and S. Bhattacharya, *Comparative modal analysis of monopile and jacket supported offshore wind turbines including soil-structure interaction.* International Journal of Structural Stability and Dynamics, 2020. **20**(10): p. 2042016.
76. Zuo, H., K. Bi, and H. Hao, *Dynamic analyses of operating offshore wind turbines including soil-structure interaction.* Engineering Structures, 2018. **157**: p. 42-62.
77. Fitzgerald, B. and B. Basu, *Structural control of wind turbines with soil structure interaction included.* Engineering Structures, 2016. **111**: p. 131-151.
78. Dai, S., et al., *Influence of soil scour on lateral behavior of large-diameter offshore wind-turbine monopile and corresponding scour monitoring method.* Ocean Engineering, 2021. **239**: p. 109809.
79. Lin, G.-L., et al., *Experimental study on seismic vibration control of an offshore wind turbine with TMD considering soil liquefaction effect.* Marine Structures, 2021. **77**: p. 102961.

Appendix I

A1.1 Scale factors for 18 selected seismic motions

Table A-1. Scale factors of selected seismic motions

No.	RSN	Scaled factors	No.	RSN	Scaled factors
1	6	1.7192	10	900	1.8006
2	15	3.4474	11	984	4.2034
3	169	1.8987	12	1044	0.9268
4	173	2.3431	13	1107	2.5444
5	180	1.2973	14	1120	0.5334
6	182	1.4696	15	1540	3.2658
7	728	2.6204	16	1633	1.5303
8	779	0.5825	17	5618	2.3271
9	799	2.2179	18	6890	1.6975

A1.2 Time history of displacement and acceleration for investigated ground motions

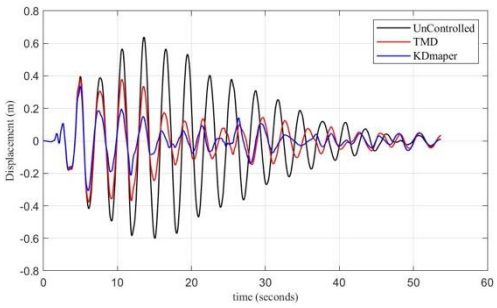

(a) No. 1

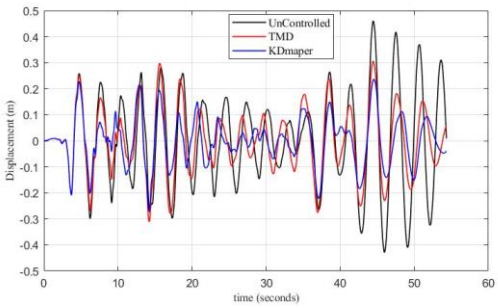

(b) No. 2

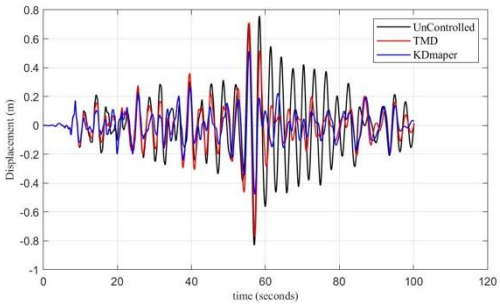

(c) No. 3

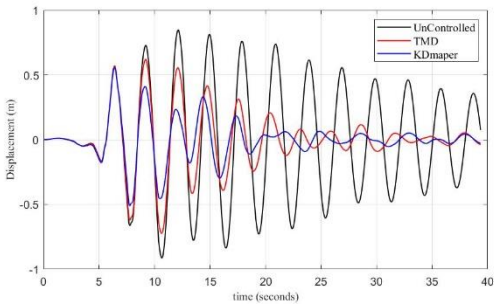

(d) No. 4

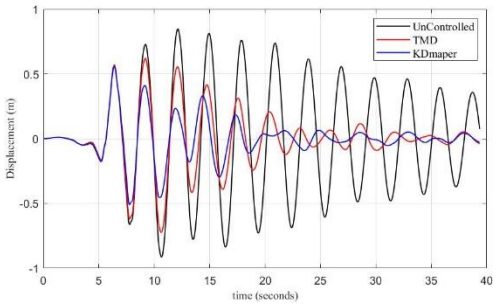

(e) No. 5

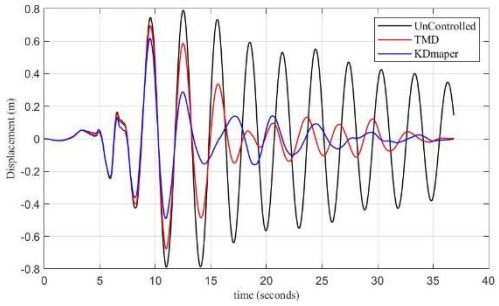

(f) No. 6

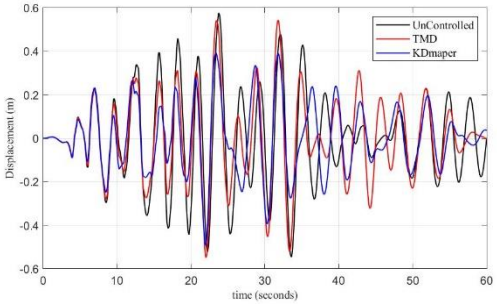

(g) No. 7

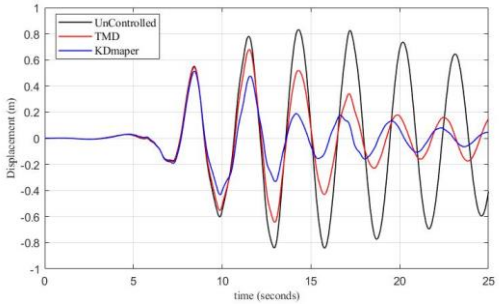

(h) No. 8

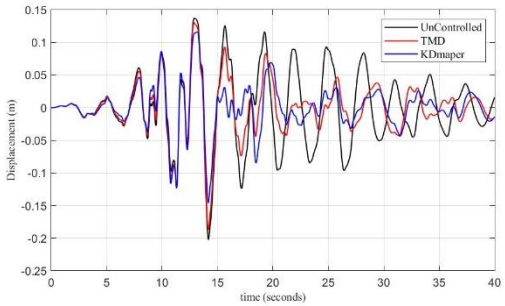

(i) No. 9

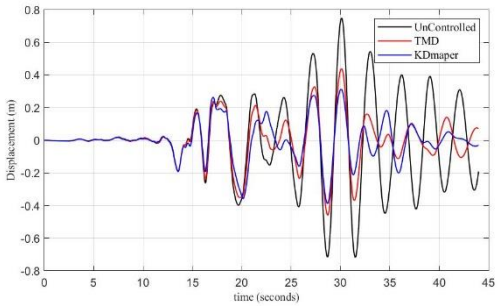

(j) No. 10

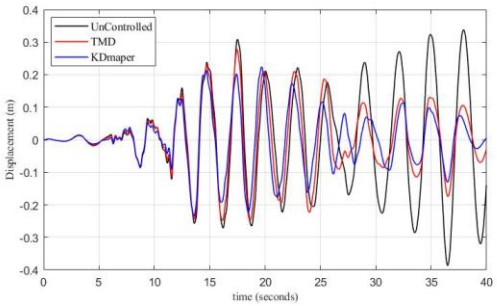

(k) No. 11

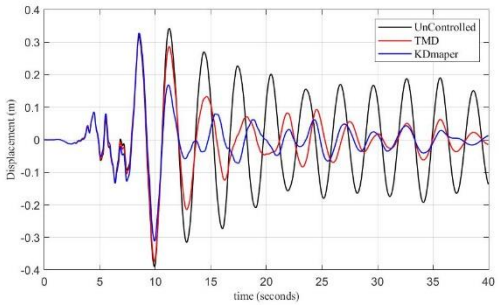

(l) No. 12

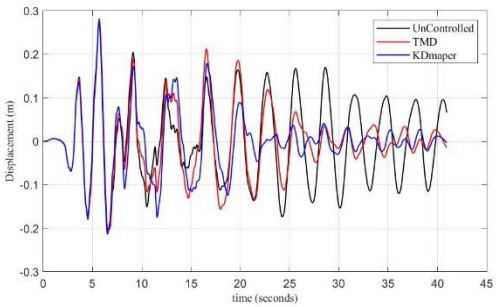

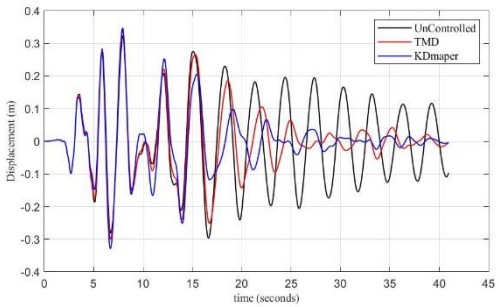

(m) No. 13

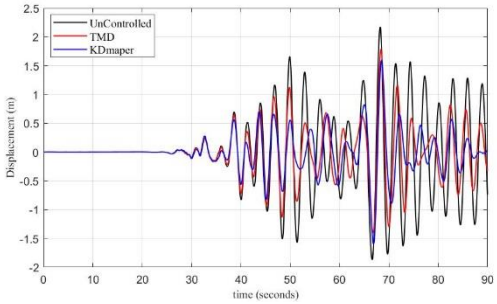

(n) No. 14

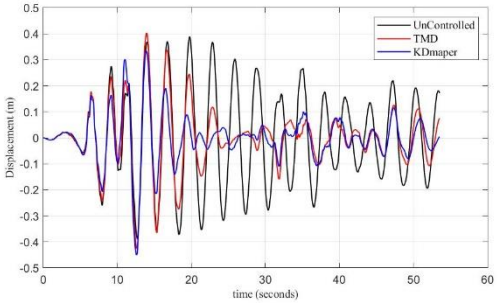

(o) No. 15

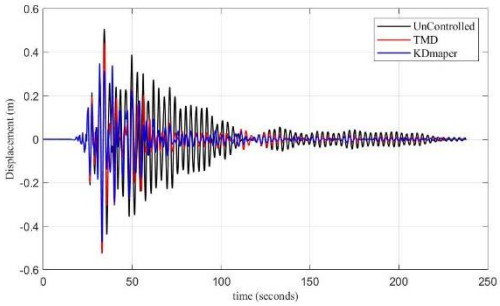

(p) No. 16

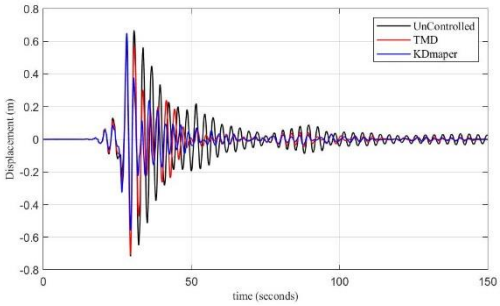

(q) No. 17

(r) No. 18

Figure A-1. Displacement time history at the tower top with and without control.

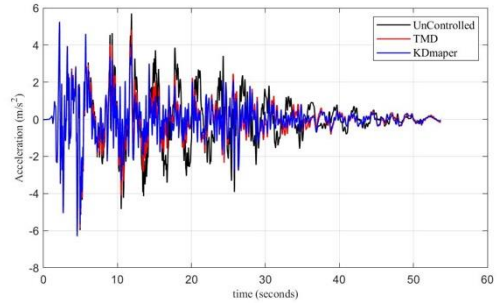

(a) No. 1

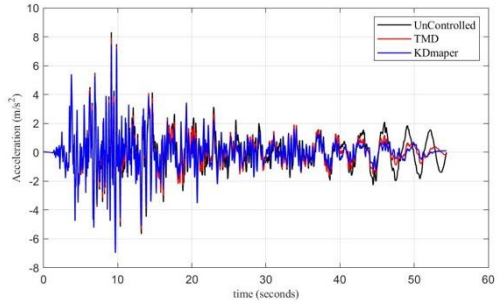

(b) No. 2

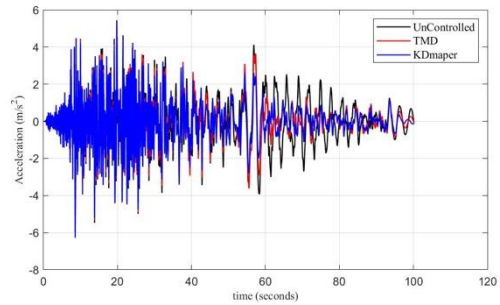

(c) No. 3

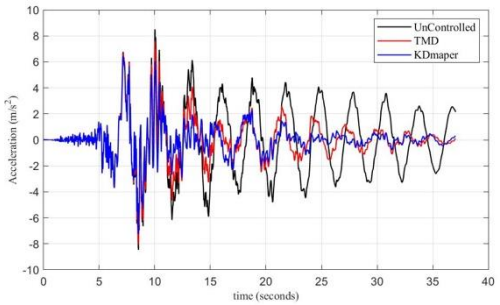

(d) No. 4

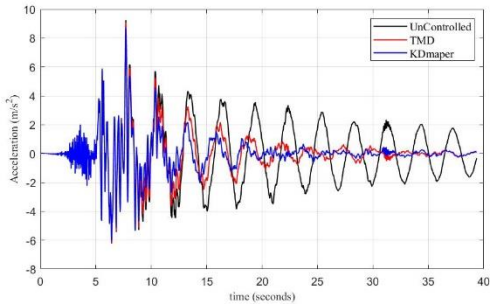

(e) No. 5

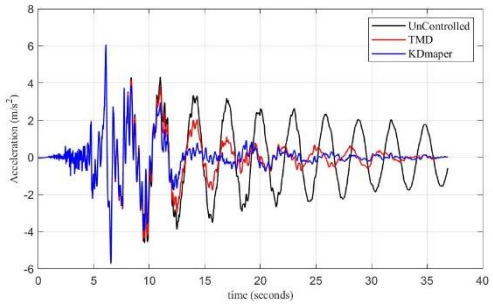

(f) No. 6

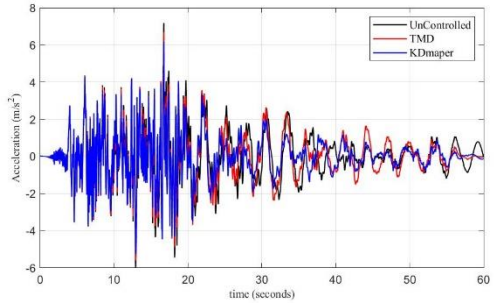

(g) No. 7

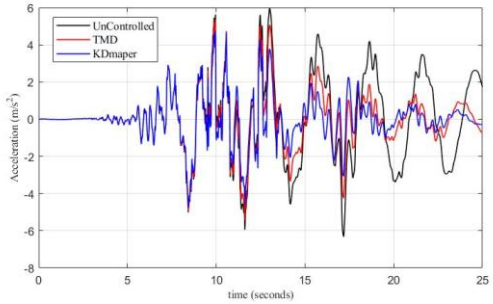

(h) No. 8

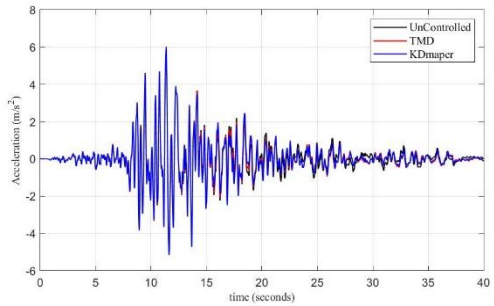

(i) No. 9

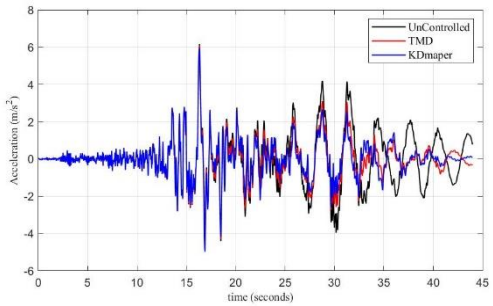

(j) No. 10

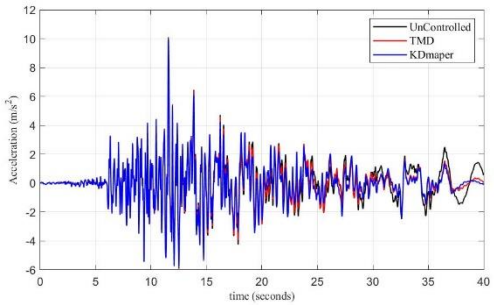

(k) No. 11

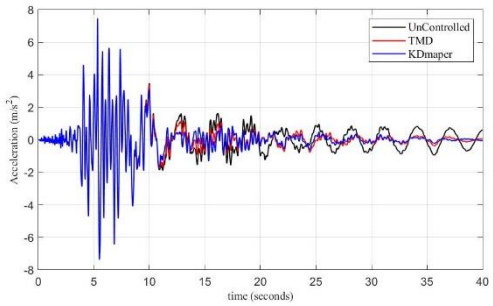

(l) No. 12

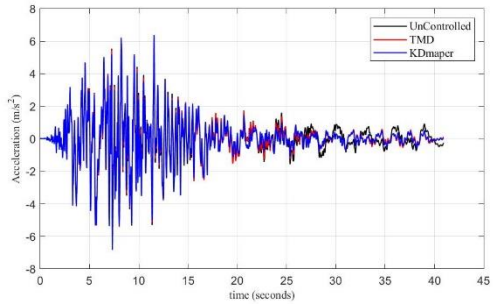

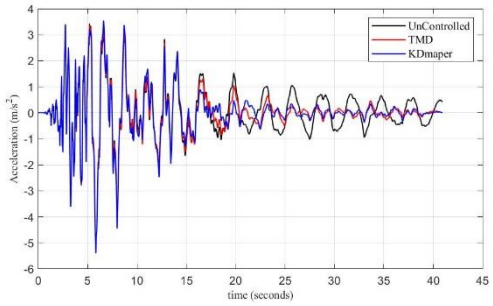

(m) No. 13

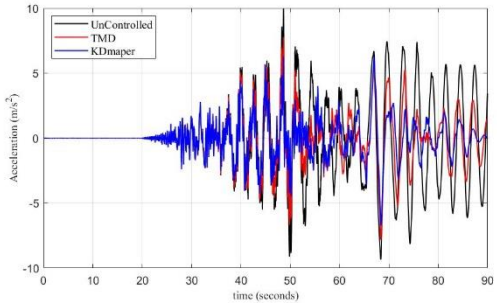

(n) No. 14

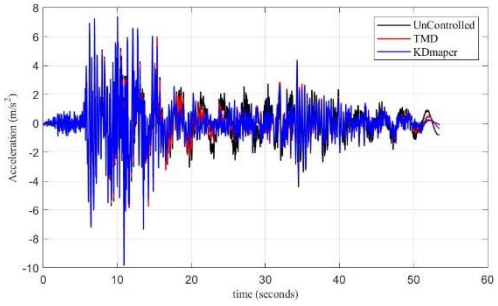

(o) No. 15

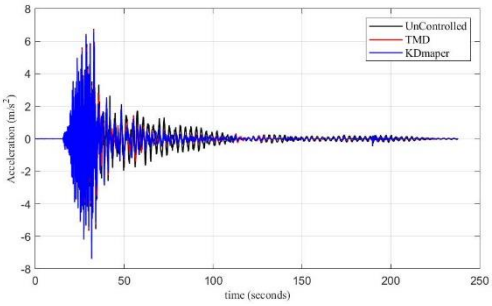

(p) No. 16

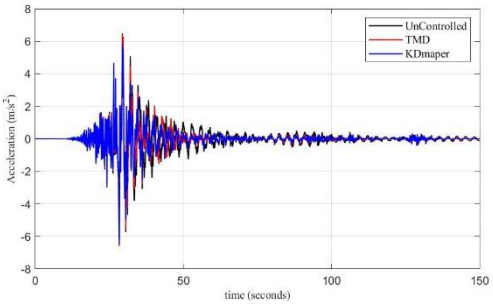

(q) No. 17

(r) No. 18

Figure A-2. Acceleration time history at the tower top with and without control

A1.3 Ratio of RMS displacement and accelerations for robustness investigation

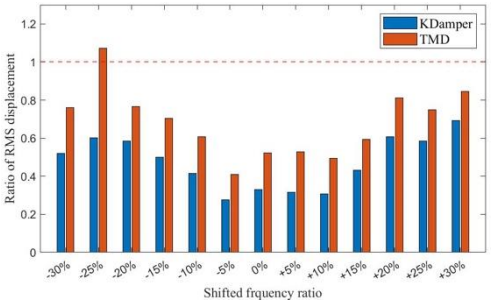

(a) No. 1

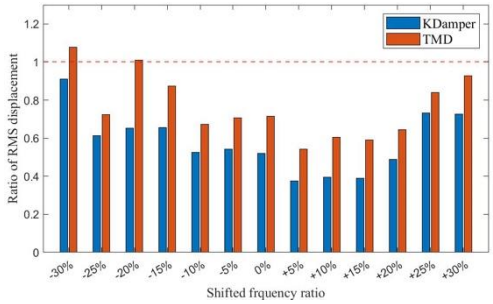

(b) No. 2

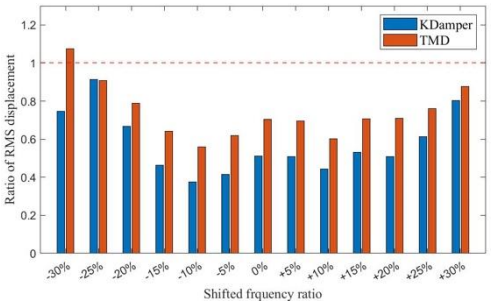

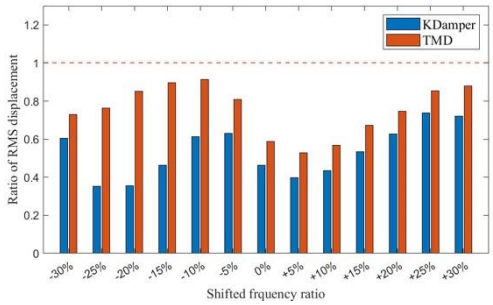

(c) No. 3

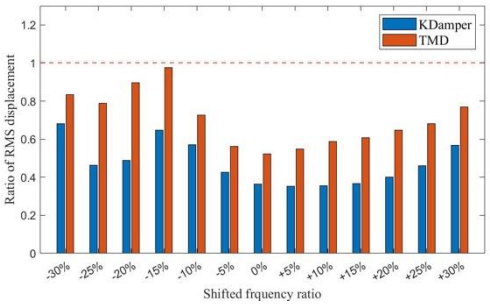

(d) No. 4

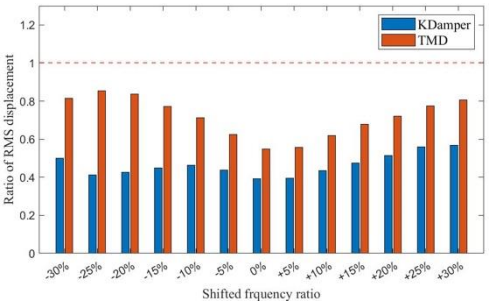

(e) No. 5

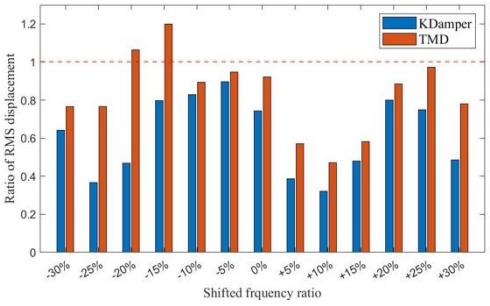

(f) No. 6

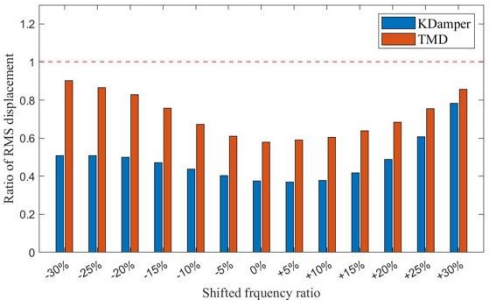

(g) No. 7

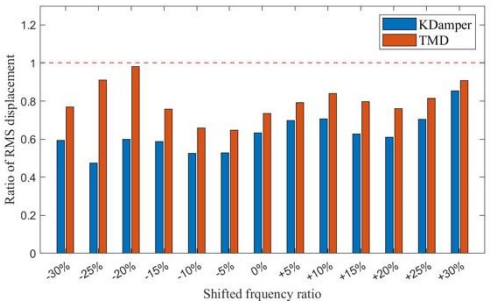

(h) No. 8

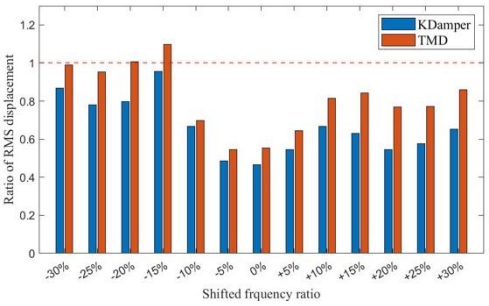

(i) No. 9

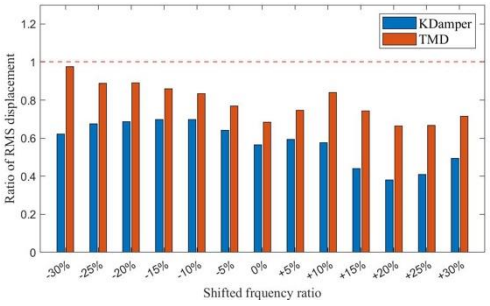

(j) No. 10

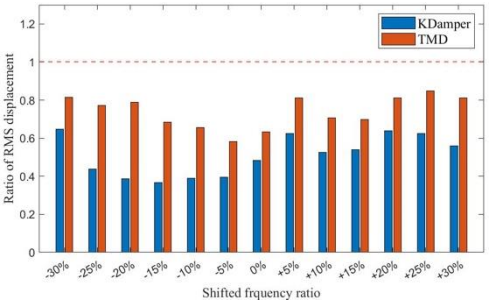

(k) No. 11

(l) No. 12

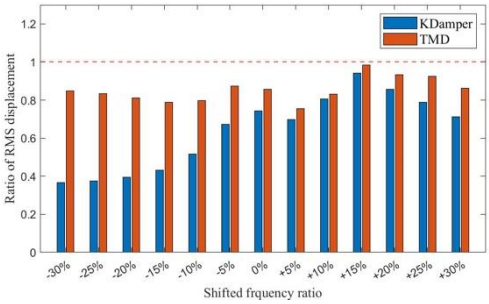

(m) No. 13

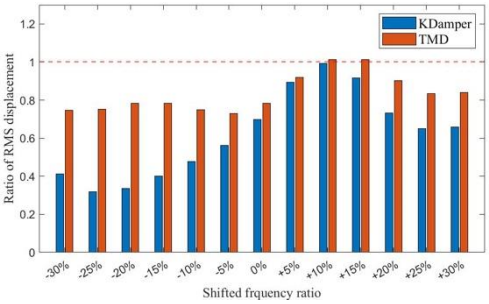

(n) No. 14

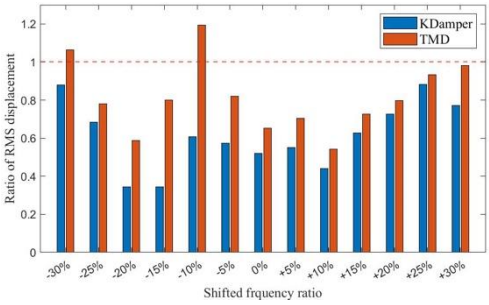

(o) No. 15

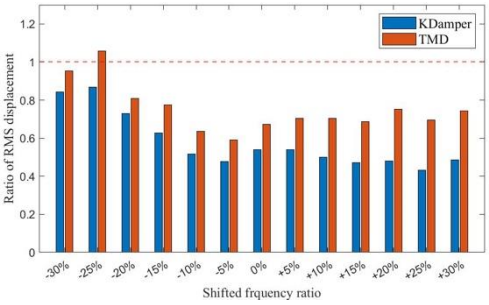

(p) No. 16

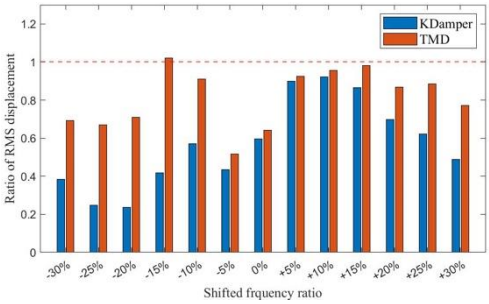

(q) No. 17

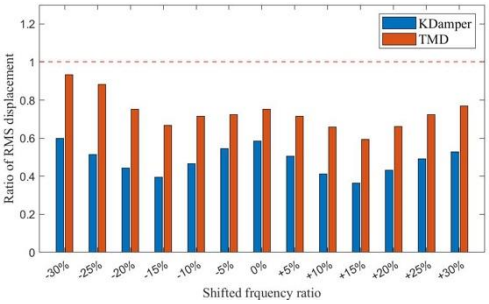

(r) No. 18

Figure A-3. Ratios of RMS displacements under different structural frequencies.

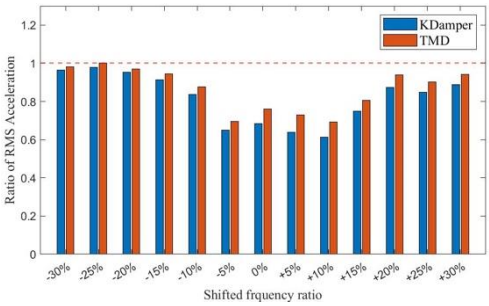

(a) No. 1

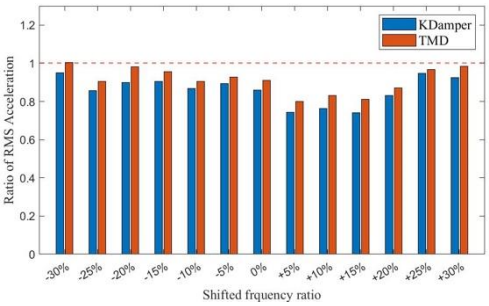

(b) No. 2

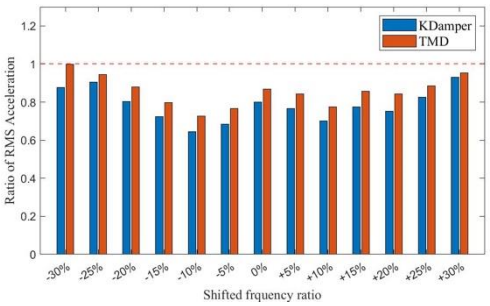

(c) No. 3

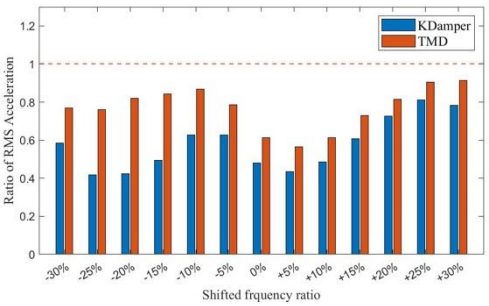

(d) No. 4

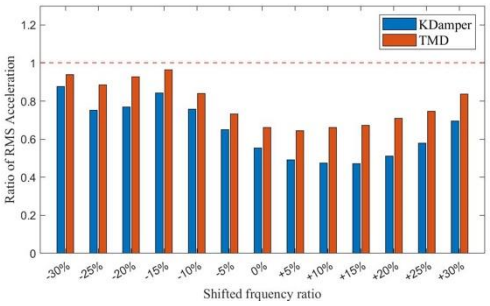

(e) No. 5

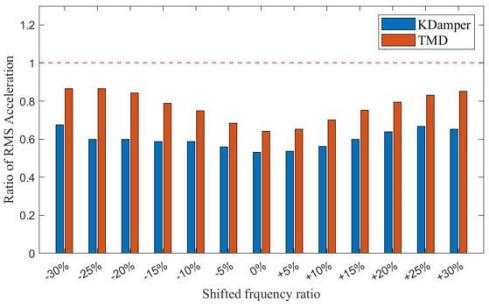

(f) No. 6

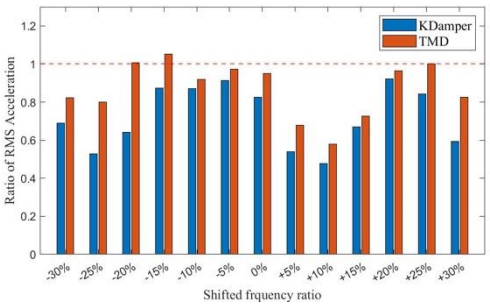

(g) No. 7

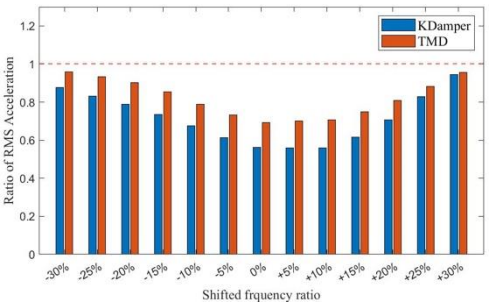

(h) No. 8

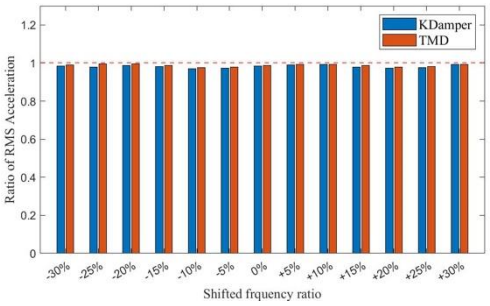

(i) No. 9

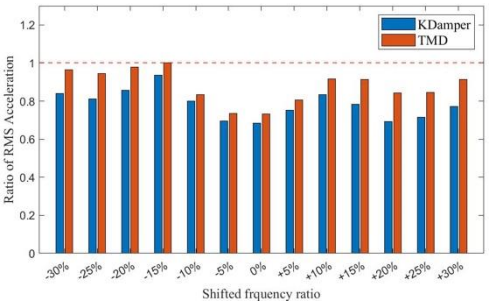

(j) No. 10

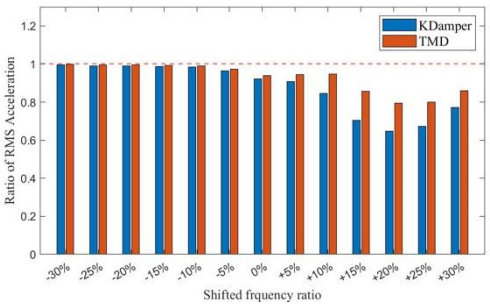

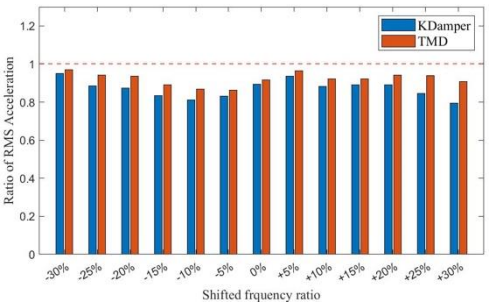

(k) No. 11

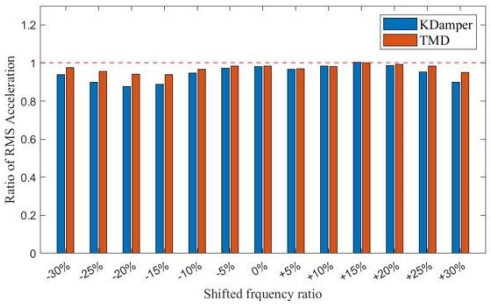

(l) No. 12

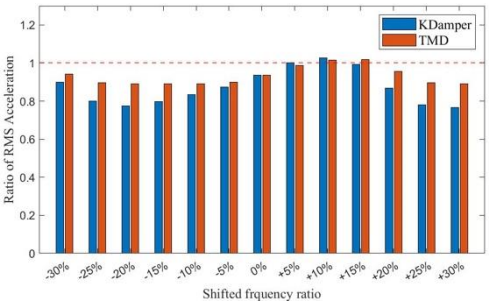

(m) No. 13

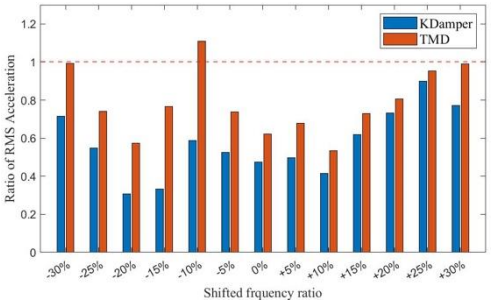

(n) No. 14

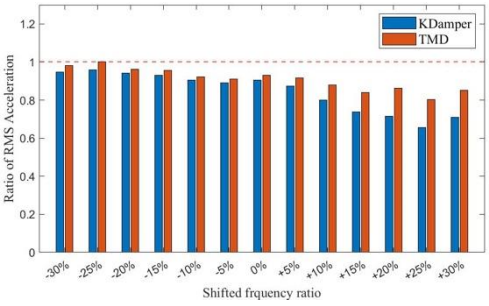

(o) No. 15

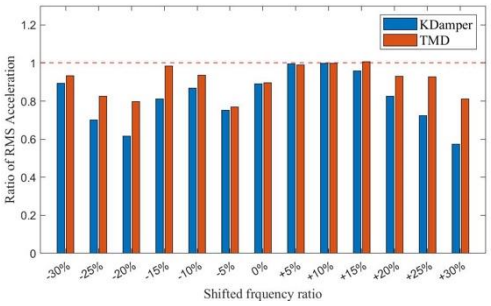

(p) No. 16

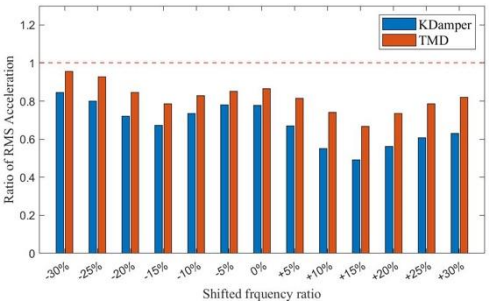

(q) No. 17

(r) No. 18

Figure A-4. Ratios of RMS accelerations under different structural frequencies